Review Article

Nano Research
2024, 17(10): 8706–8728

ISSN 1998-0124 CN 11-5974/O4
https://doi.org/10.1007/s12274-024-6853-5

Li-current collector interface in lithium metal batteries

Tian-Yu Wang, Dingyi Zhao, Keyue Liang, and Yuzhang Li (✉)

Department of Chemical and Biomolecular Engineering, University of California, Los Angeles, Los Angeles, California 90095, USA

Received: 9 April 2024 / **Revised:** 25 June 2024 / **Accepted:** 1 July 2024

ABSTRACT

Interfaces within batteries, such as the widely studied solid electrolyte interface (SEI), profoundly influence battery performance. Among these interfaces, the solid–solid interface between electrode materials and current collectors is crucial to battery performance but has received less discussion and attention. This review highlights the latest research advancements on the solid–solid interface between lithium metal (the next-generation anode) and current collectors (typically copper), focusing on factors affecting the Li-current collector interface and improvement strategies from perspectives of current collector substrate (lithiophilicity, crystal facets, mechanical properties, and topological structure), electrolyte chemistry, current density, stacking pressure, SEI, electric field and temperature, and provides a future directions and opportunities on this topic.

KEYWORDS

lithium metal anode, current collectors, Li-current collector interface, solid–solid interface, improvement strategies

1 Introduction

With the rapid development and widespread application of consumer electronics such as mobile phones and computers, electric vehicles, and intermittent renewable energy sources in the power grid (e.g., wind and solar energy), increasingly high demands have been placed on energy storage systems [1–6]. Among these, lithium-ion batteries (LIBs), as a breakthrough technology in the energy storage field, have become successful commercialized energy storage and power generation devices due to their high energy density, long cycle life, and absence of memory effect [7–10], and are widely applied in people's daily lives. A typical structure of LIBs consists of current collectors, cathodes, anodes, electrolytes, and separators [11, 12], as shown in Fig. 1(a) (illustrating the discharge process of the battery). The separator, generally made of polymers, prevents direct contact between the cathode and anode, thereby avoiding short circuits [13–15]. Current collectors connect the battery to the external circuit, allowing electrons to enter and exit the battery, with common materials including copper (typically used for the anode current collector) and aluminum (typically used for the cathode current collector) [12, 16]. The electrolyte, serving as the channel for lithium ion movement, usually comprises a mixture of lithium salts (such as lithium hexafluorophosphate ($LiPF_6$), lithium tetrafluoroborate ($LiBF_4$), etc.) and organic solvents (e.g., carbonate solvents, including ethylene carbonate (EC), dimethyl carbonate (DMC), diethyl carbonate (DEC), ethyl methyl carbonate (EMC), etc.) [11, 17, 18]. The cathode materials in commercialized LIBs primarily utilize lithium cobalt oxide ($LiCoO_2$, LCO) [19–21], ternary materials ($LiNi_xMn_yCo_{1-x-y}O_2$, NCM) [22–25], and lithium iron phosphate ($LiFePO_4$, LFP) [26–29]. Anode materials mainly consist of graphite [30–32]. In some batteries, higher capacity silicon-based anodes are also employed [33–35]. During the charging process, lithium ions intercalate between the layers of graphite forming LiC_x, while during the discharging process, lithium from LiC_x is released from the graphite as lithium ions [36–38]. However, the theoretical specific capacity of graphite anodes based on the intercalation reaction mechanism is only 372 mAh·g^{-1} [39–42], prompting researchers to develop batteries with higher performance [43–45]. Metallic lithium, with its high theoretical specific capacity (3860 mAh·g^{-1}), low chemical potential (−3.04 V, relative to the standard hydrogen electrode), and lightweight (6.94 g·mol^{-1}), has attracted widespread attention [46–48]. Batteries utilizing lithium as the anode material are referred to as lithium metal batteries (LMBs). Pairing metallic lithium anodes with cathode materials such as sulfur [49–52], air [53–55], and high-nickel ternary layered materials (e.g., $LiNi_{0.8}Co_{0.1}Mn_{0.1}O_2$, NMC811) [56–58], is expected to construct high-performance batteries with energy densities greater than 500 Wh·kg^{-1} [59–61], significantly surpassing the existing state-of-the-art commercial lithium-ion batteries (approximately 250 Wh·kg^{-1}) [62]. However, due to the uncontrollable growth of lithium dendrites and continuous parasitic reactions with the electrolyte from the highly reactive lithium metal anode, LMBs suffer from declining Coulombic efficiency (CE), cycling performance, and battery safety issues [63–65], preventing their commercialization since first proposed in the 1970s [66, 67]. Current research efforts are mainly focused on suppressing lithium dendrites and constructing a stable solid electrolyte interface (SEI) as starting points to address the challenges facing LMBs [68–73]. These efforts include modifications to the current collector [74–76], electrolyte modification (such as the use of electrolyte additives like lithium fluoride, lithium polysulfides, copper acetate, fluorides, and the development of advanced electrolytes) [77–82], and the construction of artificial SEI layers [83–85].

From the structure of batteries, it is known that there are multiple interfaces within the battery, including solid–liquid

Address correspondence to yuzhangli@ucla.edu

interfaces and solid–solid interfaces. These interfaces profoundly affect the performance of the battery and are currently a hot topic of research. For example, the SEI, which is a type of solid–liquid interface currently receiving significant attention in battery research, directly impacts the battery's cycle life, lithium deposition state, Coulombic efficiency, and safety [86]. A considerable amount of research work on SEI has been carried out, with frequent publications reviewing the latest research advancements on SEI [87, 88]. Solid–solid interfaces are common in solid-state batteries [89]. The interface between the solid electrolyte and the electrode faces issues such as high interfacial impedance, poor miscibility, and easy separation of the interface [90]. Therefore, establishing a stable solid–solid interface between components of solid-state batteries is one of the bottlenecks restricting the development of solid-state batteries and has attracted widespread attention [39].

However, there is another very important but less discussed solid–solid interface in batteries, that is, the interface between electrode materials and current collectors. The Li-current collector interface refers to the contact surface between lithium metal and the conductive current collector surface within the battery during the charge and discharge processes. In lithium metal batteries, the Li-current collector interface is a critical area because it involves the electrochemical reactions and physical deposition of lithium ions. This interface serves as the channel through which the external circuit transfers charge to the lithium metal. During charging, lithium ions are reduced to metallic lithium on the current collector surface; during discharging, metallic lithium oxidizes back to lithium ions and is released into the electrolyte. Ideally, the Li-current collector interface should form a dense and uniform lithium deposition layer. However, if the interface between lithium and the current collector is fragile—for example, due to poor contact during the deposition process—this can lead to poor deposition morphology, such as dendritic growth. It can also cause electrical disconnection between lithium and the current collector during the subsequent stripping process. This disconnection prevents lithium from gaining or losing electrons to participate in the electrochemical process, thereby resulting in the formation of "dead" lithium [91–95]. This can cause low Coulombic efficiency, short cycle life, or even damage to the battery [96–99], as shown in Fig. 1(b). More importantly, this challenge is actually quite common, as it can be caused by a variety of factors. For example, recent studies have shown that when the current density is so high that the deposition rate surpasses the formation of the SEI, the shape of lithium metal deposition is a rhombohedral dodecahedron. Moreover, this deposition shape is independent of the electrolyte chemistry and the substrate of the current collector, indicating that the intrinsic morphology of lithium metal deposition is dodecahedral [100]. As shown in Fig. 1(b), the contact between this rhombohedral dodecahedron and the current collector is almost point contact, which easily leads to the formation of dead lithium [100–102]. Therefore, achieving a dense and uniform lithium deposition structure at the Li-current collector interface is crucial. Enhancement strategies can focus on various aspects such as the initial stage of lithium deposition (nucleation), growth, thickness and morphology control, and interface reactions to obtain the ideal Li-current collector interface structure. Unfortunately, the current understanding of the interface between lithium and the current collector is limited and not extensively researched. Only a few of studies have employed characterization methods such as scanning electron microscopy (SEM) or transmission electron microscopy (TEM) to qualitatively assess the morphology of lithium deposition on the surface of the current collector. These studies often consider the absence of dendritic or fibrous lithium as evidence of performance improvement [103]. However, there is a lack of quantitative research on the contact quality between lithium and the current collector.

Therefore, this article provides a comprehensive review of the Li-current collector interface, an important solid–solid interface in batteries. It introduces the latest research progress on this critical issue and aims to stimulate researchers' attention and discussion on this topic. This review is primarily based on the latest research achievements in the past three years, introducing and analyzing factors affecting the physical contact between lithium and the current collector, and provides an outlook for future developments.

2 Factors affecting the Li-current collector interface and improvement strategies

2.1 Current collector substrate

The current collector is a crucial component of LMBs, not only connecting the anode material to the external circuit but also serving as the substrate for lithium deposition. Therefore, the

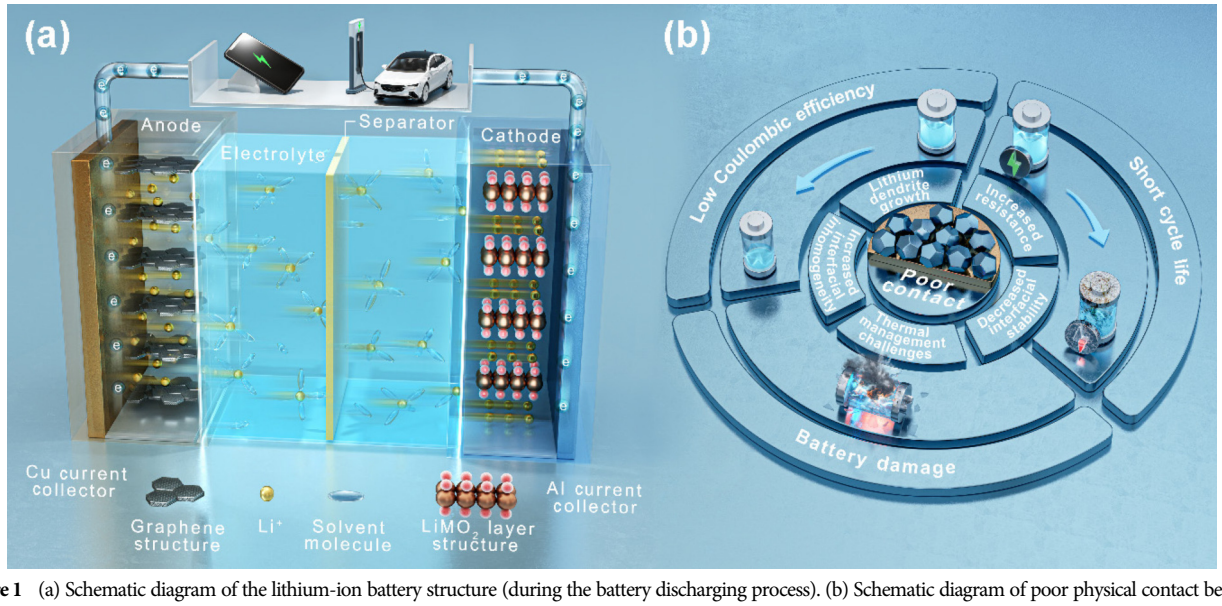

Figure 1 (a) Schematic diagram of the lithium-ion battery structure (during the battery discharging process). (b) Schematic diagram of poor physical contact between lithium and the current collector in lithium metal batteries and the potential hazards this poor contact may pose to the battery.

characteristics of the current collector substrate directly affect lithium nucleation, growth, and the contact between lithium and the current collector [3]. This section reviews the influence of the current collector's lithiophilicity, crystal facets, mechanical properties, and topological structure on the contact between lithium and the current collector, and presents potentially viable strategies for improving contact based on existing research findings.

2.1.1 *Lithiophilicity of the current collector substrate*

During the charging process of LMBs, lithium ions migrate towards the anode under the influence of electric and concentration fields, obtaining electrons on the surface of the current collector and nucleating randomly. Subsequent lithium ions are reduced at these nucleation sites and continue to grow [104]. The nucleation and early growth process of lithium significantly affects the final morphology of lithium deposition [103, 105], and different types of substrates significantly influence the lithium nucleation process. In addition to the most common copper (Cu) substrate, Yan et al. investigated substrates made of different elemental materials such as gold (Au), silver (Ag), zinc (Zn), and magnesium (Mg). They found that the energy barrier for lithium nucleation (nucleation overpotential) varies among different types of substrates [106]. For example, gold has virtually no nucleation overpotential, while copper exhibits a higher nucleation overpotential. Therefore, when both copper and gold are present as substrates, lithium deposits on gold rather than copper, thereby achieving selective deposition of lithium (as shown in Fig. 2(a)) [106]. Consequently, some studies have induced the directed nucleation and deposition of lithium by

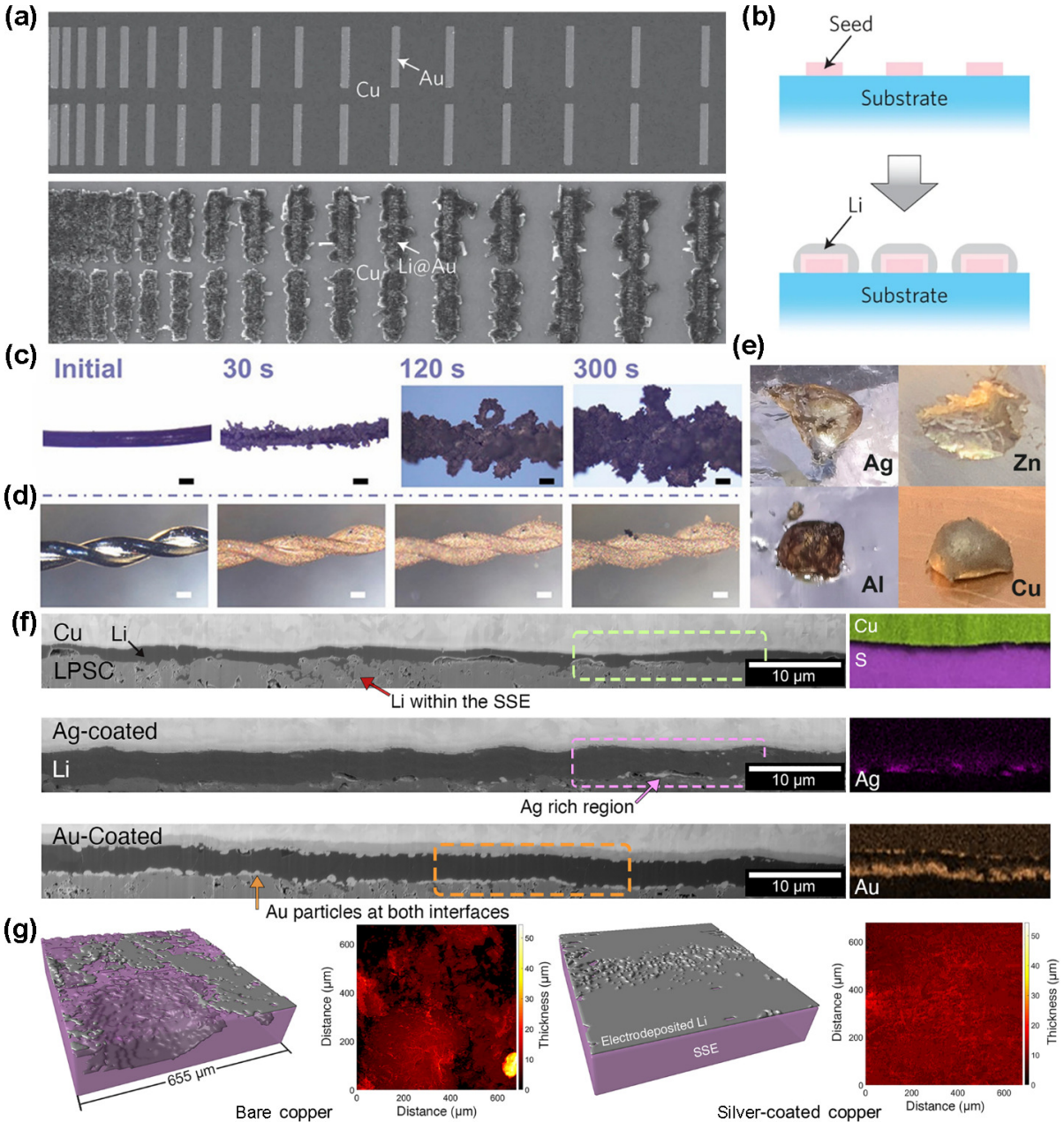

Figure 2 Lithiophilicity of the current collector substrate affects the Li-current collector interface. (a) When both copper and gold are present in the substrate, lithium selectively deposits on the gold surface with a low nucleation overpotential. (b) Schematic illustration of inducing directed nucleation and deposition of lithium using materials with low nucleation overpotentials as seeds. Reproduced with permission from Ref. [106], © Springer Nature Limited 2016. (c) Morphology of lithium deposited on the surface of non-lithiophilic copper wire and (d) lithiophilic silver wire (scale bar = 100 μm). (e) Molten lithium droplets on the surfaces of Ag, Zn, Al, and Cu foils, respectively. Reproduced with permission from Ref. [110], © American Chemical Society 2021. (f) SEM images of lithium deposited on bare copper, silver-coated copper, and gold-coated copper, respectively, from top to bottom. (g) Three-dimensional structure and deposition thickness of lithium deposited on bare copper and copper after silver coating. Reproduced with permission from Ref. [114], © Elsevier Inc. 2023.

using materials with low nucleation overpotentials as seeds (as shown in Fig. 2(b)). For instance, silver nanowires (NWs) with low nucleation overpotentials were applied on graphene [107]; aluminum (Al) with low nucleation overpotentials was used on copper current collectors to induce directed lithium deposition [108]; and gold nanoparticles were guided in hollow carbon spheres to direct lithium deposition, thereby inhibiting the growth of lithium dendrites [106].

Although materials with low nucleation overpotentials can achieve selective deposition of lithium, the contact conditions between different types of substrates and lithium still need further confirmation. For example, Fig. 2(a) qualitatively demonstrates that when copper and gold coexist on the substrate, lithium tends to deposit on the gold surface. However, it remains uncertain whether the contact conditions during lithium deposition on gold are superior to those on copper. Todeschini et al., in their study on gold deposition, found that chromium (Cr) as a substrate exhibits good wettability, and the interdiffusion between gold and chromium forms a Cr-Au alloy, resulting in good physical contact of gold deposited on chromium [109]. Therefore, if lithium can diffuse with the substrate material to form an alloy, it may imply better contact. Yan et al.'s research indicates that the crystal structure and atomic radius of both copper and gold are significantly different from lithium, so both gold and copper should exhibit nucleation barriers. However, in reality, the nucleation overpotential of gold is virtually zero, which is due to the solubility between gold and lithium and the formation of alloys [106]. Chen et al. found that lithium preferentially form alloys with lithiophilic metals. These alloy sites become the initial nucleation sites for lithium deposition, continuously adsorbing lithium ions and transferring them to the internal alloy solid phase through diffusion channels [110]. Moreover, they believe that reduced nucleation overpotentials are conducive to forming dense lithium deposits [111]. As shown in Figs. 2(c) and 2(d), lithium deposited on non-lithiophilic, high nucleation overpotential copper wires forms a large amount of lithium dendrites accompanied by significant volume expansion. However, lithiophilic silver wires under the same deposition capacity exhibit a dense deposition morphology. The color change of silver wires to yellow during deposition implies that lithium diffuses into the lattice of silver to form the Li_8Ag_5 alloy [110]. The wettability of molten lithium with the substrate can be rapidly and effectively screened for lithiophilic current collector substrates that are easy to form alloys with lithium. As shown in Fig. 2(e), after dropping molten lithium onto the substrate surface, the contact angle with silver and zinc foils is almost zero, indicating that lithium can wet silver and zinc well. The contact angle with aluminum foil is less than 90°, indicating that lithium can partially wet aluminum. However, the contact angle with copper is close to 180°, showing non-wetting characteristics [110]. The results of this experiment are also consistent with the results of lithium nucleation overpotential tests and the results of binding energy analysis based on density functional theory (DFT) calculations [106, 110].

Ma et al. constructed nucleation sites by using lithiophilic zinc to form a Li/LiZn layer. By employing graphene oxide, which can stabilize zinc as a nucleating seed, they achieved uniform and smooth deposition and extraction of lithium, suppressing the formation of dead lithium and dendrites [112]. Wang et al. prepared a current collector modified with tellurium copper (Te-Cu). The Te-Cu current collector forms a lithiophilic Li_2Te-Cu coating in the activation process with Li, resulting in a very uniform and dense deposition morphology on the modified current collector surface, with no apparent formation of dead lithium during the process of lithium deposition/dissolution [113]. Sandoval et al. in their study of anode-free solid-state batteries [114], as illustrated in Fig. 2(f), discovered that lithium deposition on the surface of copper current collectors was uneven, and the thickness of lithium deposited on the current collector's surface was significantly lower than expected. This was attributed to a considerable amount of lithium growing into the pores of the solid-state electrolyte (SSE). After coating the copper current collector surface with a 100-nm lithiophilic layer of silver or gold, lithium deposition became more uniform, the thickness approached theoretical values, and almost no lithium growth was observed in the pores of the SSE. This finding was further verified by three-dimensional (3D) structural images of lithium deposition obtained through synchrotron X-ray microcomputed tomography (μCT) measurements. As shown in Fig. 2(g), the shape of lithium deposited on bare copper was uneven, with significant height variations and a large amount of lithium growing into the pores of the SSE. However, after applying a silver coating, the shape and height of lithium deposition were more uniform, and no lithium growth was observed inside the SSE (note that this image is designed to show lithium growth in the SSE, hence lithium is shown below the SSE rather than the current collector, but the morphology of lithium also reflects the deposition morphology on the current collector surface) [114]. They believed that the improvement in contact after coating with lithiophilic layers could be attributed to two reasons. First, the low nucleation overpotential of the lithiophilic coating promoted the formation of a dense and uniform lithium deposition layer, and the uniform lithium layer had good contact with the current collector during stripping, thus reducing isolated areas and cavity formation during the stripping process. Second, the coating could locally release lithium through a dealloying reaction at the end of stripping and increasing current density [114]. Although the alloying reaction of lithiophilic metal substrates (such as Ag, Au, and Zn foils) can drive diffused lithium ions into the bulk phase, resulting in a desirable deposition morphology, repeated electrochemical cycles gradually coat the substrate surface with lithium. This process ultimately leads to a deposition of lithium on the substrate surface that is loose, porous, and poorly contacted [115, 116]. Therefore, Li et al. proposed a lithiophilic LiHg thin film. Given that Hg has a diffusion coefficient in lithium-rich solutions that is 10–20 orders of magnitude greater than that of Ag, Au, and Zn, the LiHg alloy thin film was able to maintain dense lithium deposition and smooth contact with the substrate even at a high deposition capacity of 55 $mAh{\cdot}cm^{-2}$, whereas traditional lithiophilic metal substrates exhibited loose, porous lithium deposition morphology at a deposition capacity of 5 $mAh{\cdot}cm^{-2}$ under the same test conditions [115].

In addition to the metals that can form alloys with lithium mentioned above, inorganic materials that can generate mixed ion-electron conductors through conversion reactions with lithium (such as ZnO, SiO_2, CuO, CuP, MgF_2, etc.) are also lithiophilic materials that can be used to improve the contact between lithium and the current collector [117, 118]. For example, Zou et al. reported a lithiophilic substrate with a core–shell structure, S-CuNW, and observed the process of uniform nucleation and dense deposition of lithium through characterization techniques such as *in situ* transmission electron microscopy, optical microscopy, X-ray photoelectron spectroscopy (XPS), etc [118]. Liu et al. pre-grew an ultra-thin and dense layer of metallic lithium seeds on the surface of copper current collectors to increase lithiophilicity, achieving dense deposition of lithium and significantly enhancing the physical bonding strength between lithium and the current collector [119]. Wang et al. prepared a ZnS-ZnO nanotube-modified 3D carbon cloth current collector, where ZnS and ZnO as precursors formed LiZn alloy increased lithiophilicity and induced uniform nucleation and deposition of

lithium [120]. Zhang et al. used carbon cloth as a substrate, introduced Co nanoparticles onto the surface of nitrogen-doped carbon nanotubes (NCNTs), and constructed a three-dimensional lithiophilic framework, achieving uniform lithium deposition [121]. He et al. constructed a lithiophilic SiO_x/C@C core–shell structure to modify copper foil. The highly lithiophilic SiO_x/C core prompts initial lithium deposition within the shell cavity. Subsequently, the lithiophilic C shell, doped with N and S, facilitates uniform lithium deposition across the shell gaps. Finally, facilitated by a uniform conductive network, lithium achieves a uniform and dense deposition on the copper substrate [116]. However, contrary to the widely accepted approach of constructing lithiophilic surfaces, Wu et al. adopted a lithophobic surface by depositing hexagonal crystals prepared from a LiF and Fe nanoparticle composite. Due to the fast lateral diffusion rate of lithium on this surface, it promoted the gradual deposition of polyhedra to form a dense, almost porosity-free layer of lithium [122]. Although this approach can inhibit the growth of lithium dendrites, the polyhedral shape is difficult to form tight contact with the current collector [100, 101].

In summary, the nucleation and early growth processes of lithium significantly affect the final morphology of lithium deposition, and different types of current collector substrates influence the Li-current collector interface by affecting the lithium nucleation process. Lithiophilic substrates that form alloys with lithium, such as gold, silver, and zinc, have low nucleation overpotentials, which favor dense lithium deposition on the current collector surface and ensure better contact quality between lithium and the current collector [123]. Therefore, improving the Li-current collector interface can be achieved by using lithiophilic materials for the current collector substrate (metals or inorganic materials), coating lithiophilic layers, or creating lithiophilic nucleation sites.

2.1.2 *Crystal facets*

The crystal facets of the substrate can influence the electrodeposition process of lithium [124, 125], thereby affecting the adhesion and contact between lithium and the current collector. Kim et al. deposited lithium on copper foil containing (115) grains in a (111) orientation, with results shown in Fig. 3(a) [126]. The observation reveals that the amount of lithium deposited at the grain boundaries significantly exceeds that inside the grains, with a greater deposition on (115) grains compared to (111) grains, each displaying distinct deposition morphologies. Needle-shaped depositions appear on (115) grains, whereas (111) facets show rhombohedral dodecahedral particles. First-principles calculations reveal that the migration barrier for lithium atoms on the copper (111) surface is almost zero, which promotes lithium growth along two-dimensional planes rather than three-dimensional dendritic growth, as shown in Fig. 3(b). With increasing deposition time, these rhombohedral dodecahedral lithium particles gradually aggregate and interconnect to form two-dimensional lithium islands [126]. However, as shown in Fig. 3(c), whether it be rhombohedral dodecahedral lithium particles or the lithium islands they form through interconnection, only partial contact is made with the (111) copper foil current collector, and the adhesion between them is not strong [126]. Zhang et al. achieved the crystal facet control of lithium deposition on copper substrates

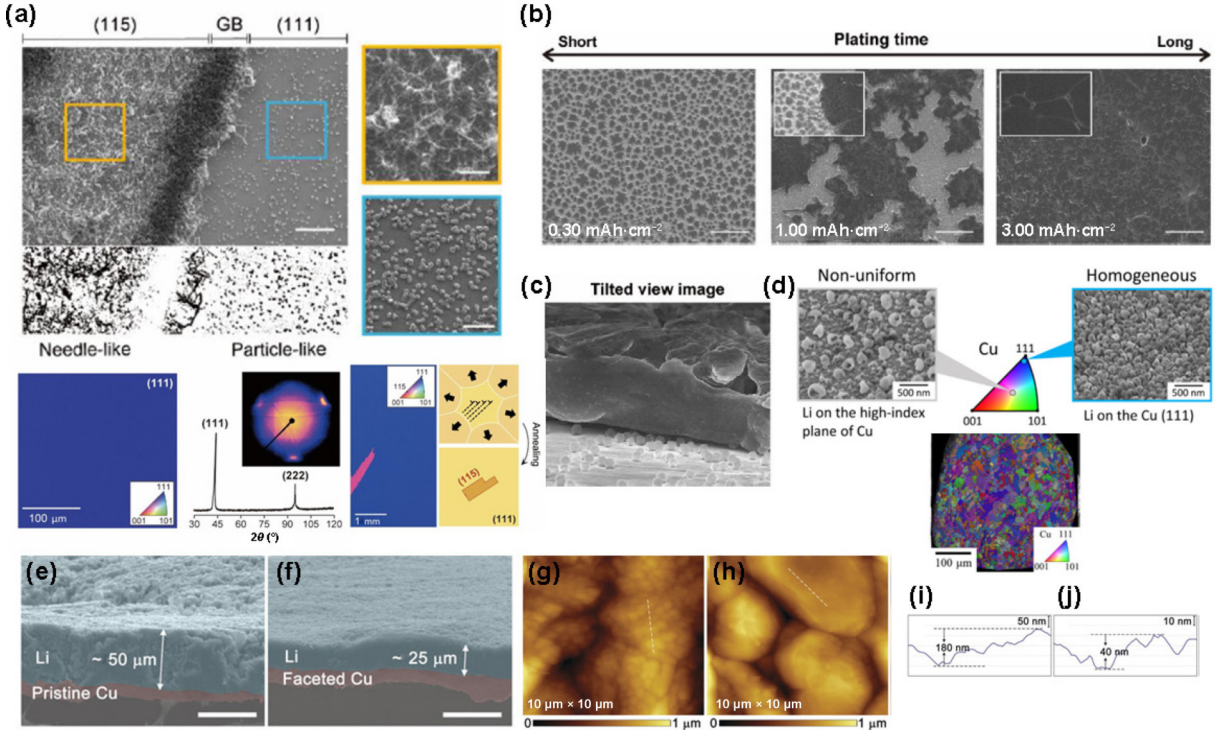

Figure 3 Crystal facets of the current collector substrate affects the Li-current collector interface. (a) SEM images (top) of lithium deposited on (111) copper foil with (115) grains. Scale bars: the large image on the left is 20 μm, and the small image on the right is 5 μm. Characterization of single crystal Cu (111) foils (lower left) and Cu (111) foil embedded with (115) twin grains (lower right) by electron backscatter diffraction (EBSD) analysis. (b) Top-view SEM images of lithium deposited on (111) monocrystalline copper foil at capacities of 0.30, 1.00, and 3.00 mAh·cm^{-2} (scale bar = 100 μm). (c) A 70° oblique view SEM image of lithium deposited on (111) monocrystalline copper foil at a capacity of 3.00 mAh·cm^{-2} (scale bar = 5 μm). Reproduced with permission from Ref. [126], © Kim, M. H. et al. 2022. (d) SEM images (top) of lithium deposition on polycrystalline copper current collectors shows the smallest size and most uniform distribution of lithium on copper grains with orientations close to (111). Crystal orientation map obtained by EBSD analysis (bottom). Reproduced with permission from Ref. [129], © American Chemical Society 2017. SEM images of lithium deposited on (e) copper current collectors and (f) copper foils with a (100) preferential orientation facet (scale bar = 50 μm), AFM surface morphology images of (g) copper current collectors and (h) copper foils with a (100) preferential orientation facet, and localized smoothness of (i) copper current collectors and (j) copper foils with a (100) preferential orientation facet. Reproduced with permission from Ref. [132], © Wiley-VCH Verlag GmbH & Co. KGaA, Weinheim 2019.

using LaF_3 nanoparticles, changing the preferred growth facet of lithium from (110) to (200), leading to two-dimensional growth, resulting in dense and smooth deposition of lithium on the current collector surface [127]. Lai et al. conducted large-scale molecular dynamics simulations of the lithium-copper interface based on a high-accuracy neural network potential field, discovering that lithium exhibits different potential energy distributions and dynamic characteristics on copper surfaces with different crystal facets. Moreover, the deposition on (111) and (100) surfaces was very flat and uniform, significantly superior to that on the (110) surface [128].

Ishikawa et al. conducted lithium electro-deposition on polycrystalline copper current collectors and discovered that lithium deposited on copper grains with orientations close to (111) had the smallest size and most uniform distribution as shown in Fig. 3(d). Numerical analysis indicated that the dependence of atomic concentration on crystal orientation at equilibrium has a significant impact on morphology changes during the initial stages of electro-deposition [129]. Furthermore, they also found that the SEI's formation is closely related to the crystal facets of the current collector, with traditional polycrystalline copper current collectors leading to uneven formation of SEI, whereas the SEI formed on monocrystalline copper (111) current collectors exhibited the smallest thickness and resistance [130]. However, Kim et al. reported different results [131]. They electro-deposited lithium on monocrystalline copper current collectors with (100), (110), and (111) orientations and found that the (100) copper substrate had the lowest nucleation overpotential, and lithium selectively deposited on the (100) planes on polycrystalline copper foil. The (100) copper foil exhibited more dense and uniform lithium nucleation sites, thereby doubling the cycle stability of lithium deposition or dissolution. Gu et al. held a similar view, finding that copper (100) exhibited lithiophilicity [132]. As shown in Figs. 3(e) and 3(f), compared to the loose deposition morphology of lithium on the original copper current collector surface, the deposition morphology on the (100) copper foil was denser, with the latter's deposition thickness being only half of the former's under the same deposition capacity. SEM images also showed tighter contact between lithium and the (100) copper foil compared to the original copper foil. Moreover, atomic force microscopy (AFM) characterization indicated that the deposition morphology of lithium on the (100) copper foil surface was smoother (Figs. 3(g)–3(j)).

In summary, current research through experiments and calculations has found that different crystal facets affect the migration barriers and lithiophilicity of lithium atoms on the surface of the current collector. For example, the migration barrier of lithium atoms on the Cu (111) surface is almost zero, promoting two-dimensional planar growth rather than three-dimensional dendritic growth. The Cu (100) substrate has the lowest nucleation overpotential and shows denser and more uniform lithium nucleation sites. However, more mechanistic studies are still needed to resolve the existing controversies and find the optimal option for which crystal facet yields the best effect.

2.1.3 *Mechanical properties*

The mechanical properties of the substrate can influence the characteristics of the deposited layer [133], representing a parameter that is easily overlooked but significantly impacts the deposition process. For example, Luo et al. demonstrated that the deposition rate of stable high-density glass on soft substrates is ten million times faster than on hard substrates for glass of the same properties [133]. In LMBs, there are residual stresses present during the lithium electro-deposition process, and if these stresses cannot be timely relieved, they will affect the final morphology of the deposition. Therefore, Wang et al. proposed a stress-driven lithium growth model [134]. As shown in Figs. 4(a) and 4(b), if traditional hard substrates are used, the residual stresses during lithium deposition cannot be released, potentially causing poor contact between lithium and the current collector and the formation of lithium dendrites. However, if soft substrates are used, the substrate can continuously release the residual stresses during lithium deposition by forming wrinkles, thereby inhibiting the formation of lithium dendrites. Experimental results also confirmed this idea, as shown in Fig. 4(c), after 1 h of electro-deposition, lithium exhibited a loose, filamentous deposition morphology on the surface of traditional hard copper current collectors. Then, polydimethylsiloxane (PDMS) was used as a soft substrate with a thin copper film attached to prepare soft copper current collectors. After electro-deposition for the same duration, as shown in Fig. 4(d), the deposited lithium tightly and smoothly covered the surface of the current collector, exhibiting better contact conditions than with hard current collectors [134].

Oh et al. attached a lithiophilic magnesium thin film to the current collector to achieve stable lithium nucleation and inserted a soft MXene layer beneath the magnesium film (as shown in Fig. 4(e)) to buffer stress. The authors analyzed the modified mechanical properties using nanoindentation techniques and found that the indentation depth after inserting the flexible MXene layer increased by seven times compared to those without the MXene layer, demonstrating superior ductility. Then, high-resolution three-dimensional structural characterization was performed using a three-dimensional X-ray microscopy (XRM) and a computed tomography (CT) system. As shown in Fig. 4(f), severe contact loss occurred with only the magnesium film, with an internal porosity reaching 28%, and the interface between the magnesium film and the electrolyte was rough. In contrast, as shown in Fig. 4(g), when a soft MXene layer was inserted beneath the magnesium film, the MXene layer acted to release stress, resulting in smoother contact, an internal porosity of only 6%, and a flat interface between the magnesium film and the electrolyte [135].

In summary, residual stress exists during the lithium deposition process. Using soft current collectors can continuously release the residual stress generated during lithium deposition by creating wrinkles, leading to better contact and thus a more ideal Li-current collector interface.

2.1.4 *Topological structure*

Since the commercialization of LIBs, planar copper foils have been widely used as current collectors for the anode due to their outstanding conductivity, stability, and ease of processing [136]. However, the planar shape of copper foils, with their low specific surface area and high local current density, coupled with the inevitable presence of defects during preparation that can act as "hotspots" for lithium nucleation and growth with low charge transfer impedance, can lead to a fragile Li-current collector interface. This results in the formation of dead lithium, capacity fading, and constraints on further development of batteries [3]. Therefore, modifying the topological structure of the current collector to increase the specific surface area and reduce local current density has become an effective way to address this issue. For example, copper meshes, due to their lower current density and more uniform charge distribution, lead to uniform and smooth deposition of lithium [137], thus exhibiting better cycling performance than planar copper foil current collectors [138]. Furthermore, three-dimensional current collectors with higher specific surface areas have attracted broader attention. The pore size, pore volume, and electroactive surface area ratio (i.e., the area

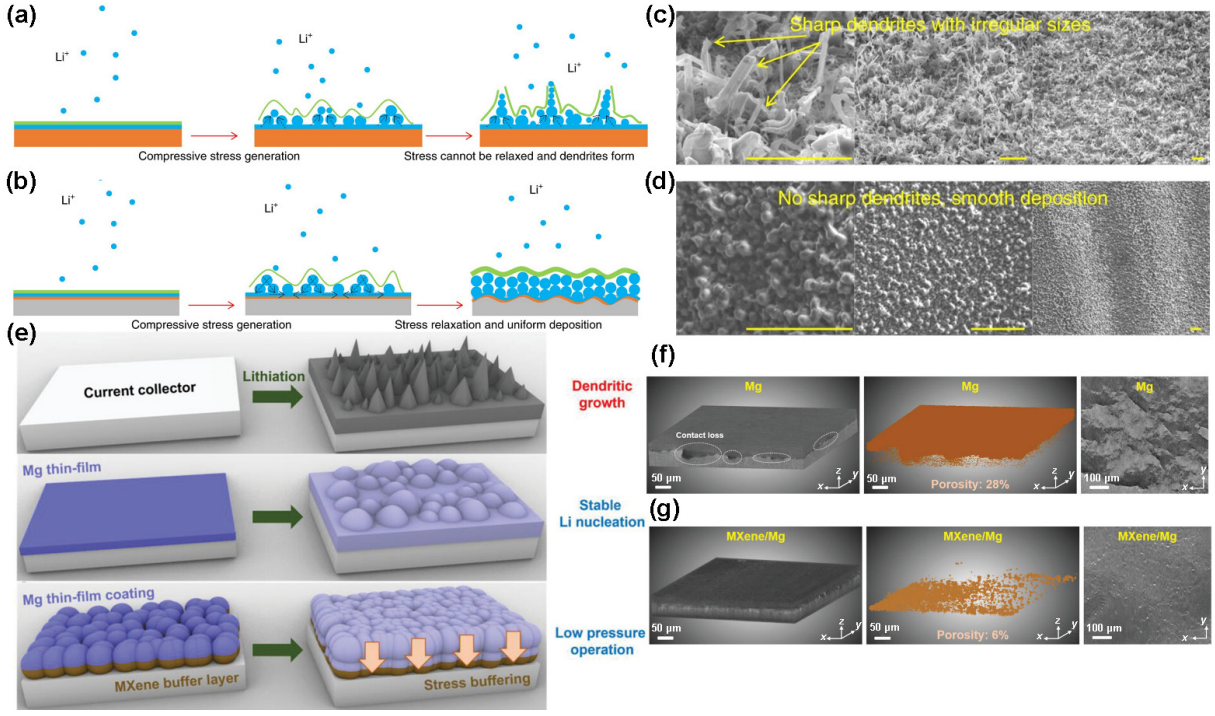

Figure 4 Mechanical Properties of the current collector substrate affects the Li-current collector interface. Stress is generated during lithium deposition, where (a) hard substrates cannot release stress, while (b) soft substrates can form wrinkles to release this stress. In the diagram, green, blue, orange, and gray respectively represent SEI, lithium, copper current collector, and soft materials (such as PDMS). (c) Lithium exhibits a loose, filamentous deposition morphology on the surface of hard copper current collectors, (d) Lithium tightly and smoothly covers the surface of the current collector. Reproduced with permission from Ref. [134], © Wang, X. et al. 2018. (e) Schematic illustration of lithium deposition on a pure current collector, a current collector coated with a lithiophilic magnesium thin film, and further addition of a soft MXene layer. (f) Characterization results of the three-dimensional XRM and computed tomography (CT) system with only the magnesium film coated, and (g) after adding a soft MXene layer beneath the magnesium film. Reproduced with permission from Ref. [135], © Wiley-VCH GmbH 2023.

of the current collector that can come into contact with the electrolyte) are important indicators for 3D current collectors [139]. Smaller pore sizes (sub-micron level) provide a larger specific surface area and lower local current density, thereby promoting dense deposition of lithium. A larger pore volume allows the 3D structure of the current collector to accommodate more lithium. A higher electroactive surface area ratio facilitates lithium deposition within the internal structure of the 3D current collector rather than on the surface (as shown in Fig. 5(a)), providing a larger contact area between lithium and the current collector, which is beneficial for improving the reversibility of the lithium plating/stripping process [139]. As shown in Figs. 5(b) and 5(c), after depositing the same capacity of lithium, lithium is loosely deposited on the surface of planar copper foils. In contrast, in 3D current collectors, a large amount of lithium is densely deposited within the three-dimensional structure, fitting well with the pores and effectively increasing the contact area between lithium and the current collector [140]. By observing the deposition process of lithium in the 3D current collector, as shown in Fig. 5(d), it is evident that the internal structure of the 3D current collector has numerous uniformly distributed nucleation sites, leading to uniform nucleation and growth of lithium [140]. Therefore, designing 3D current collectors with high pore volume to electroactive surface area ratio and pore size play a significant role in improving the Li-current collector interface. Below, we introduce both metallic and non-metallic current collectors with three-dimensional topological structures.

2.1.4.1 Three-dimensional metallic current collectors

Metallic (such as copper) current collectors, due to their performance advantages and cost-effectiveness, are the most widely used commercial current collectors. Therefore, modifying the topological structure of metal current collectors to construct three-dimensional metallic current collectors has garnered widespread attention, with the challenges and costs primarily related to how to build 3D structures. Common methods include templating, chemical reduction, and scalable electro-deposition.

The templating method involves depositing a metal substrate on an organic or inorganic template via electrochemical methods, then removing the template to obtain a 3D structure. It is an attractive method for constructing 3D metallic current collectors. Park et al. used polylactic acid (PLA) particles as a template to prepare porous copper current collectors, as illustrated in Fig. 5(e). Figures 5(f) and 5(g) show the SEM images before and after removing the template from the copper deposited on the template. This 3D copper current collector promotes uniform lithium deposition and exhibits the same effect at higher current densities, indicating that the improvement in the Li-current collector interface by the 3D copper current collector is independent of current density [140]. Tang et al. used polymethyl methacrylate (PMMA) microspheres as a template to prepare 3D copper current collectors via electrophoresis. They found that lithium tends to deposit in areas of the current collector pores with a high radius of curvature (high electric field intensity) [136]. Additionally, PDMS [141], NaCl powder [142], and hydrogen bubbles [143] can also be used as templates to prepare three-dimensional current collectors for a better Li-current collector interface.

The redox method involves oxidizing the current collector and then reducing it, building a 3D current collector in the process from oxidation to reduction. Yang et al. immersed flat copper foil in ammonia water to deposit $Cu(OH)_2$, dehydrated it to CuO, and finally reduced it to obtain a copper current collector with a three-dimensional structure, as shown in Fig. 5(h). The prepared three-dimensional porous current collector is shown in Fig. 5(i). After depositing 2 $mAh{\cdot}cm^{-2}$ of lithium, dense and compact lithium deposition can be observed within the current collector (Fig. 5(j)). The high electroactive surface area provided good contact,

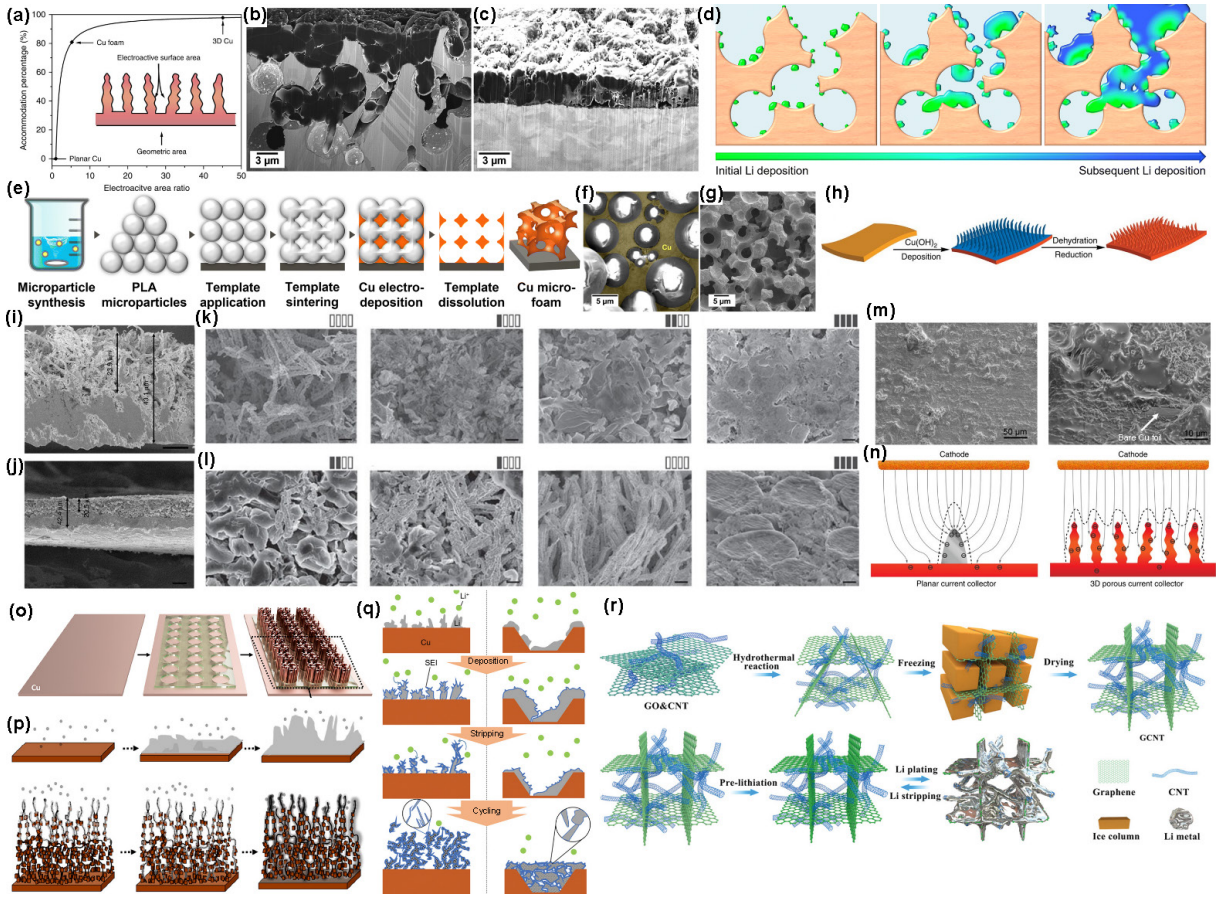

Figure 5 The topological structure of current collectors affects the Li-current collector interface. (a) The relationship between the percentage of lithium deposited inside the internal structure of current collectors with different topological structures to the total deposited amount and the electroactive surface area ratio. Reproduced with permission from Ref. [139], © Yang, C. P. et al. 2015. Cross-sectional SEM images of lithium deposited on (b) copper foam and (c) planar copper foil (current density: 0.1 mA·cm^{-2}, capacity: 0.20 mAh·cm^{-2}). (d) A schematic diagram of continuous growth of lithium within the pores of the copper foam current collector. (e) Schematic diagram of preparing a 3D copper current collector via a templating method. SEM images of a 3D copper current collector successfully prepared by electrodepositing copper on a PLA template, before (f) and after (g) removal of the PLA template. Reproduced with permission from Ref. [140], © Ingber, T. T. K. et al. 2023. (h) Schematic diagram of preparing a 3D copper current collector via a redox method. (i) SEM image of a 3D porous current collector and (j) cross-sectional SEM image after lithium deposition in the 3D porous current collector (capacity: 2 mAh·cm^{-2}, scale bar = 20 μm). (k) Top views of lithium deposition in the three-dimensional porous current collector at capacities of 0, 0.5, 1, and 2 mAh·cm^{-2} (from left to right), and (l) side views of the lithium anode after stripping 1, 1.5, and 2 mAh·cm^{-2} and after 10 cycles (from left to right) (scale bar = 2 μm). (m) Top (left) and side (right) SEM views after depositing 2 mAh·cm^{-2} of lithium on a planar current collector. (n) Schematic diagram of electrochemical deposition of lithium on planar (left) and three-dimensional porous (right) current collectors. Reproduced with permission from Ref. [139], © Yang, C. P. et al. 2015. (o) Schematic diagram of preparing a porous 3D Cu-CNT current collector. (p) Schematic diagram of lithium plating/stripping on planar copper foil (top) and 3D Cu-CNT composite current collector (bottom). Reproduced with permission from Ref. [146], © Park, S. K. et al. 2023. (q) Schematic diagram of lithium deposition on a 2D copper current collector (left) and a copper current collector with a 2.5D microstructure (right). Reproduced with permission from Ref. [147], © Yang, I. et al. 2022. (r) The preparation process and lithium deposition behavior on a 3D graphene/carbon nanotube composite current collector. Reproduced with permission from Ref. [161], © Wiley-VCH GmbH 2021.

allowing the lithium plating and stripping process to be well-controlled with good reversibility. After numerous charging and discharging cycles, the lithium anode maintains a flat surface, making dendrite formation difficult (Figs. 5(k) and 5(l)). However, as shown in Fig. 5(m), after depositing 2 mAh·cm^{-2} of lithium, a large amount of protruding moss-like deposition was observed on the planar current collector. They believed that for planar current collectors, lithium nucleates and deposits on smooth surfaces, leading to increased local electric field intensity at the tips, causing subsequent lithium to deposit and grow along the tips and form dendrites. But the sub-micron scaffold of the three-dimensional porous current collector has numerous protrusions, thus providing a large number of nucleation sites that enable uniform lithium deposition within the three-dimensional porous current collector, making the overall electric field distribution uniform and forming a flat lithium deposition surface, as shown in Fig. 5(n). Adair et al. oxidized the copper current collector substrate to form $Cu(OH)_2$ with a three-dimensional nanowire structure and then reduced it to obtain a three-dimensional nanowire copper current collector. They believed this process enhanced the lithiophilicity of copper, promoting alloying between lithium and copper during the deposition process [144]. Lin et al. through the redox method, prepared a copper framework current collector with an internal mesh structure, finding that this current collector could significantly improve Coulombic efficiency [145].

To meet the needs of large-scale commercial production, methods that can achieve high-throughput preparation of three-dimensional current collectors (such as scalable electro-deposition) have attracted attention. For instance, as shown in Fig. 5(o), Park et al. electroplated copper metal with CNTs to prepare a Cu-CNT composite current collector with a three-dimensional structure. This approach allows flexible adjustment of the current collector's pore volume (by changing thickness), porosity, etc., thus holding potential for large-scale preparation. They observed the deposition and stripping process of lithium on planar copper foil and 3D Cu-CNT current collectors, finding that lithium could fully contact the 3D Cu-CNT current collector and thus have a good deposition morphology (Fig. 5(p)), and maintaining 99%

Coulombic efficiency after 800 cycles using a half-cell [146]. Yang et al., through photolithography combined with electrodeposition, prepared a copper current collector with a two-and-a-half dimensional (2.5D) microstructure. As shown in Fig. 5(q), for planar copper current collectors, lithium tends to form porous, moss-like deposits. During the deposition and stripping process, the non-conductive SEI layer can cause lithium to lose electrical connection with the current collector and form dead lithium. The current collector with a 2.5D microstructure allows lithium to merge within limited micro-cavities, establishing a good electrical link with each other and the current collector, effectively suppressing the accumulation of dead lithium [147].

Moreover, other methods exist to obtain metal current collectors with three-dimensional topological structures, such as alloying two metals and then constructing a three-dimensional topological structure through de-alloying [148, 149]. Although constructing metal current collectors with three-dimensional structures can improve the contact between lithium and the current collector compared to planar ones, the relatively weak lithiophilicity of the current collectors (especially copper) suggests there is still significant room for improvement in achieving a more perfect Li-current collector interface. Therefore, introducing lithiophilic sites to obtain a better Li-current collector interface while constructing three-dimensional current collectors can be adopted, as reviewed in Section 2.1.1. For example, lithiophilic (such as lithiophilic metals Ag, Zn, Au, etc., and metal oxides CuO, ZnO, etc.) coatings [150, 151], nanoparticles [152, 153], lithium fluoride (LiF) [154], etc., can be introduced on the surface layer of the three-dimensional current collector.

2.1.4.2 Three-dimensional carbon-based current collectors

Although three-dimensional metallic current collectors offer advantages like enhanced performance, cost-effectiveness, and processing ease, facilitating a superior Li-current collector interface to commercial planar copper foil, their high density poses a challenge to the development of high-performance batteries. The weight of commercially used copper foil current collectors accounts for more than 10% of the total weight of LIBs [155]. Therefore, in recent years, frameworks formed by interconnecting networks based on carbon materials, such as carbon fibers, carbon nanotubes, graphene, carbon cloth, and their derivatives, have attracted increasing attention [156–159].

Song et al. deposited an Mg_3N_2 nanolayer on the surface of three-dimensional carbon foam (CF) via chemical vapor deposition (CVD) and found that lithium could be deposited uniformly and densely on the carbon framework [160]. Yang et al. constructed a material with a three-dimensional porous structure using layers of graphene and carbon nanotubes, as shown in Fig. 5(r). Its large specific surface area and high electrical conductivity network facilitated smooth growth of lithium during the deposition process, gradually filling the internal spaces with increasing deposition capacity, and exhibited good reversibility [161]. Pan et al. constructed lithiophilic three-dimensional carbon-based current collectors with low nucleation overpotential carbon defects *in situ* on three-dimensional carbon paper. This current collector promoted smooth lithium deposition and improved reversibility and cycle stability [162].

In conclusion, modifying the topology of the current collector and constructing three-dimensional current collectors to increase specific surface area and reduce local current density is a key method for obtaining a better Li-current collector interface [163]. Key factors include the pore size, pore volume, and electroactive surface area ratio of the 3D current collectors. Submicron-sized small pores provide larger specific surface area and lower local current density, promoting denser lithium deposition. Larger pore volumes allow the 3D structure of the current collector to accommodate more lithium. A higher electroactive surface area ratio facilitates lithium deposition within the internal structure of the 3D current collector rather than just on the surface, resulting in a larger contact area between lithium and the current collector, which enhances the reversibility of the lithium plating/stripping process. Besides commonly used metal current collectors, the use of lightweight carbon materials with 3D topologies is gaining more attention. Furthermore, introducing lithiophilic sites into the 3D current collector can achieve a more perfect Li-current collector interface.

The current collector directly influences the Li-current collector interface. Further analysis of existing research conclusions reveals that the current collector mainly affects the Li-current collector interface by impacting the lithium deposition process. For example, the nucleation process of lithium is influenced by the nucleation overpotential of the substrate. Lithiophilic current collector substrates that easily form alloys with lithium (such as gold, silver, and zinc) facilitate the formation of dense lithium deposits on the current collector surface and achieve better contact quality between lithium and the current collector. Additionally, low current densities favor dense lithium deposition. Therefore, constructing three-dimensional current collectors to increase specific surface area and reduce local current density is an important means of obtaining a better Li-current collector interface. However, the above studies on the Li-current collector interface mainly use SEM or TEM for qualitative characterization of the interface between lithium and the current collector, lacking quantitative research. This absence of quantitative criteria makes it difficult to directly compare different research findings. Consequently, while there are qualitative conclusions about which parameters of the current collector affect the Li-current collector interface, it is challenging to establish quantitative evaluation standards. Even among different papers, conclusions, such as which crystal facet of the current collector leads to the best Li-current collector interface, are sometimes contradictory. Therefore, developing new characterization methods and quantitatively analyzing the impact of various conditions of the current collector on the Li-current collector interface (such as area and strength) are crucial.

2.2 Electrolyte chemistry

The electrolyte chemistry directly alters the deposition process of lithium in LMBs and has a crucial impact on the Li-current collector interface [164]. For example, as shown in Fig. 6(a) [100], filamentous [165], rod-like [166], columnar [167], and blocky [168] deposition morphologies can be presented in four different electrolytes, leading to different contact conditions. Factors such as the solvation strength and concentration of the electrolyte may influence the Li-current collector interface. For instance, Boyle et al., based on ultramicroelectrodes and electrochemical impedance spectroscopy (EIS), revealed the mechanism by which the electrolyte influences the morphology of lithium deposition. The results indicated that weak solvation with rapid charge transfer induces a higher Li surface energy, favorable for uniform deposition of large lithium blocks. In contrast, strong solvation leads to the opposite effect, favoring high surface area deposition, which may result in lithium dendrites (as shown in Fig. 6(b)) [164]. Kim et al. developed a new weakly solvating electrolyte that maintains a good deposition morphology and reversibility of lithium plating and stripping after multiple cycles [169]. Ma et al. proposed that weak solvation enhances the reversibility of lithium deposition/stripping, resulting in improved contact between lithium and the current collector at low temperatures (−40 °C) (as shown in Fig. 6(c)) [170].

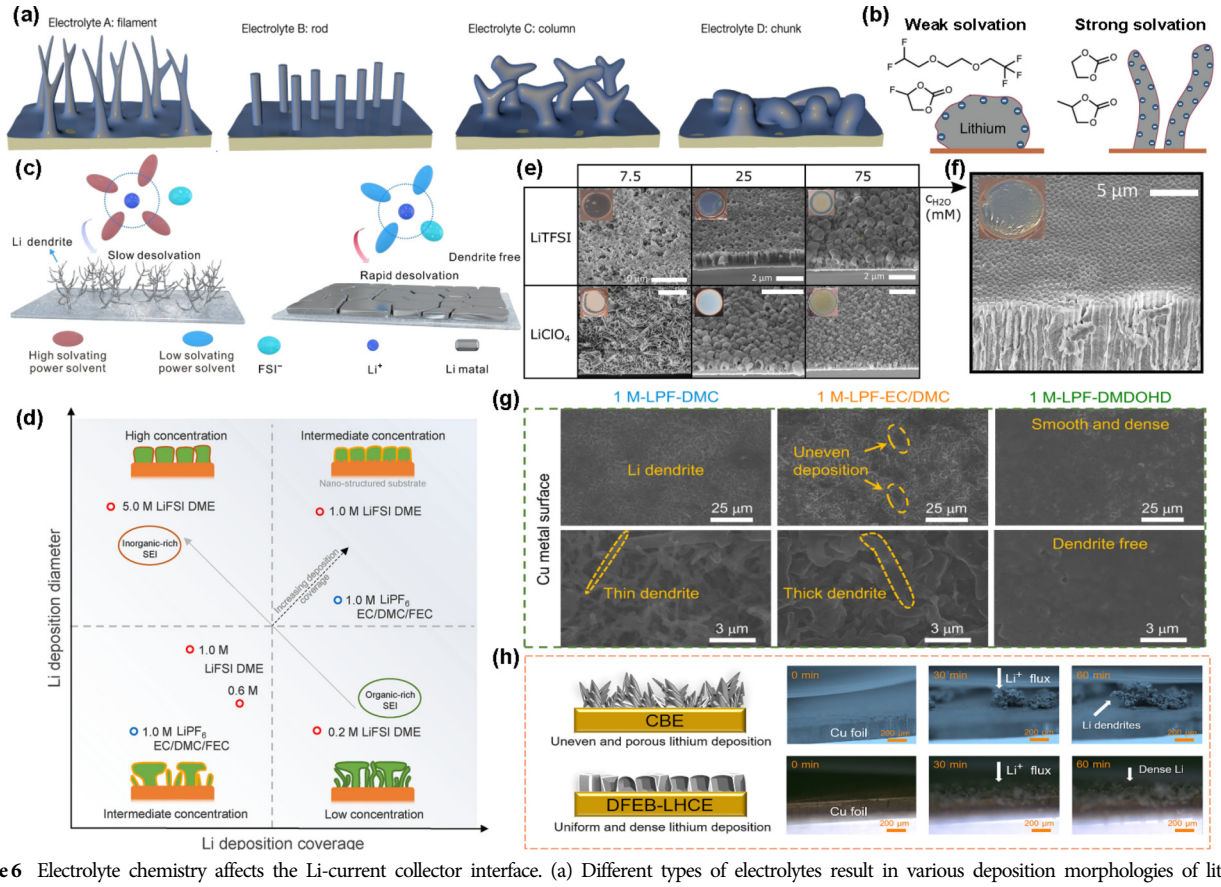

Figure 6 Electrolyte chemistry affects the Li-current collector interface. (a) Different types of electrolytes result in various deposition morphologies of lithium. (Electrolyte A: 1 M $LiPF_6$ in 1:1 v/v EC/DEC, Electrolyte B: 1 M $LiPF_6$ in propylene carbonate (PC) with 2 wt.% $LiAsF_6$ and 2 wt.% fluoroethylene carbonate (FEC), Electrolyte C: 0.6 M lithium difluoro (oxalate) borate (LiDFOB) and 0.6 M $LiBF_4$ in 1:1 v/v FEC/DEC, Electrolyte D: 4 M lithium bis(fluorosulfonyl)imide (LiFSI) in 1,2-dimethoxyethane (DME)). Reproduced with permission from Ref. [100], © Yuan, X. T. et al. 2023. (b) Schematic showing how the strength of electrolyte solvation affects the lithium deposition process. Reproduced with permission from Ref. [164], © American Chemical Society 2022. (c) Schematic illustrating the impact of the strength of electrolyte solvation on lithium deposition in a low-temperature (−40 °C) working environment. Reproduced with permission from Ref. [170], © Wiley-VCH GmbH 2022. (d) Schematic diagram showing the relationship between electrolyte concentration and both the coverage rate and diameter of lithium deposition. Reproduced with permission from Ref. [171], © Wang, Q. D. et al. 2022. (e) SEM images of lithium deposited from electrolytes with varying amounts of water as additive (using 4G as the solvent combined with either 1 M LiTFSI or 1 M $LiClO_4$). (f) SEM image of dense and uniform deposition of 30 μm thick lithium using LiTFSI electrolyte containing 25 mM H_2O. Reproduced with permission from Ref. [173], © American Chemical Society 2024. (g) SEM images of the copper current collector surface after lithium deposition in DMC, EC/DMC, and DMDOHD based electrolytes (current density: 0.2 mA·cm^{-2}, capacity: 1 mAh·cm^{-2}). Reproduced with permission from Ref. [174], © Zhang, X. Z. et al. 2024. (h) Morphological characteristics of lithium deposition in different electrolytes (CBE and DFEB). Reproduced with permission from Ref. [175], © American Chemical Society 2024.

Wang et al. discovered that the concentration of electrolytes could change the diameter and coverage rate of lithium deposition, thus affecting the Li-current collector interface. As illustrated in Fig. 6(d), their findings revealed that while dilute electrolytes create high deposition coverage and serve as a good starting point for dense lithium deposition, they also lead to the formation of unstable SEIs. These unstable SEIs hinder the development of large, dense lithium deposits. In contrast, high-concentration electrolytes foster stable SEIs, supporting the growth of substantial lithium deposits. However, the lower initial nucleation density with these electrolytes results in incomplete coverage of the current collector, thereby impeding dense lithium deposition. Therefore, they utilized modifications to the current collector to increase nucleation density and used medium concentration (about 1.0 M) electrolytes to achieve dense lithium deposition [171]. Chen et al. also discovered that the concentration of the electrolyte affects the morphology of lithium deposition. They found that higher electrolyte concentrations lead to a greater number and more uniform distribution of lithium nuclei, which favors the formation of dense, regularly shaped deposits without dendrites. They suggest that this is because low-concentration electrolytes form an SEI rich in organics with low interfacial energy, which cannot suppress dendrite formation. In high-concentration electrolytes, the formation of an SEI rich in inorganics with high interfacial energy necessitates a reduction in the total surface area to lower the overall interfacial energy, resulting in decreased surface area of the deposited lithium and thus a dense deposition morphology [172]. Aarts et al. pointed out that water could be directly used as an additive in electrolytes to improve lithium deposition. As shown in Fig. 6(e), they used dry tetraglyme (4G) as a solvent combined with 1 M lithium bis(trifluoromethylsulphonyl)imide (LiTFSI) or 1 M $LiClO_4$ and different amounts of water as the electrolyte, finding that as the amount of water increased, lithium gradually changed from mossy to columnar forms. Using LiTFSI electrolyte with 25 mM H_2O additive at a current density of 1 mA·cm^{-2} resulted in dense and uniform lithium deposition of 30 μm thickness, as shown in Fig. 6(f) [173].

Additionally, modifying electrolytes to improve the Li-current collector interface has attracted increasing attention. Currently used carbonate-based electrolytes (CBEs), linear carbonates (like DMC) have low viscosity and melting point but do not easily form stable SEIs on the anode, whereas cyclic carbonates (like EC) can solve this issue but have a high melting point (36.4 °C). Although merging the two can achieve co-optimization of melting point, viscosity, and interface, there still exists the problem of uncontrollable lithium deposition leading to dendrites. Therefore, Zhang et al. used an ester exchange reaction between DMC and

open-chain products of EC to form 2,5-dioxahexanedioate (DMDOHD) with two carbonate groups as the solvent. As shown in Fig. 6(g), both DMC and EC/DMC led to poor Li-current collector interfaces with large amounts of uneven, loose, and porous lithium deposition, but DMDOHD-based electrolyte enabled smooth and dense lithium deposition [174]. Zeng et al. designed a 2,3-difluoroethoxybenzene (DFEB) electrolyte, as shown in Fig. 6(h), observing dense and uniform lithium deposition on copper foil. In contrast, commercial CBE showed fluffy and porous lithium deposition on copper foil, demonstrating poor contact with the copper foil [175]. Lu et al. introduced a new solvation adjustment strategy by introducing "bulky" solvation molecules with both coordinating and non-coordinating zones, reducing the interaction between lithium ions and the solvent, thus obtaining a good lithium deposition morphology [176]. Cheng et al. adjusted the chemical composition of the electrolyte to maintain a weak solvation effect of lithium ions with higher ionic conductivity at low temperatures, thus achieving uniform and dense lithium deposition at low temperatures (–40 °C) [177]. Ma et al. designed an additive that could form an adsorption layer on the lithium metal surface to hinder the charge transfer of lithium ions, alleviating concentration polarization during the deposition process, thereby achieving good lithium deposition morphology and stable deposition/stripping cycles [178].

In summary, different types of electrolytes lead to different lithium deposition morphologies on the current collector. Weakly solvated electrolytes with rapid charge transfer induce higher lithium surface energy, while appropriately concentrated electrolytes provide a good starting point for forming high-coverage dense lithium deposition along with a stable SEI. Modifying the electrolyte composition to alter viscosity and interactions between lithium ions and solvents can also potentially result in a better Li-current collector interface.

2.3 Current density

The variation in current density changes the morphology of lithium deposition, thereby affecting the Li-current collector interface. As shown in Fig. 7(a), at a current density of 10 mA·cm^{-2}, the lithium deposition morphology is filamentous. When increased to 100 mA·cm^{-2}, non-filamentous particles appear, and at 1000 mA·cm^{-2}, lithium deposits solely in the form of rhombohedral dodecahedra [179]. As illustrated in Fig. 7(b), with the current density increasing from 50 to 150 mA·cm^{-2}, the number of deposited polyhedral lithium particles increases, while the number of dendritic lithium particles decreases. When the current density increases to 200 mA·cm^{-2}, there are no dendritic lithium particles, and further increasing to 1000 mA·cm^{-2} does not change the polyhedral shape. This indicates that beyond a certain threshold, the morphology of lithium deposition stabilizes as a polyhedral shape and remains unaffected [100]. Yuan et al. discovered that when the current density is sufficiently high to surpass the formation speed of SEI and avoid mass transfer limitations, the intrinsic deposition morphology of lithium is a rhombohedral dodecahedron, which is independent of the type of electrolyte and current collector substrate. As shown in Fig. 7(c), they found that at a current density of 1 mA·cm^{-2}, different types of electrolytes exhibited various deposition morphologies: filamentous, rod-like, columnar, and blocky. However, when the

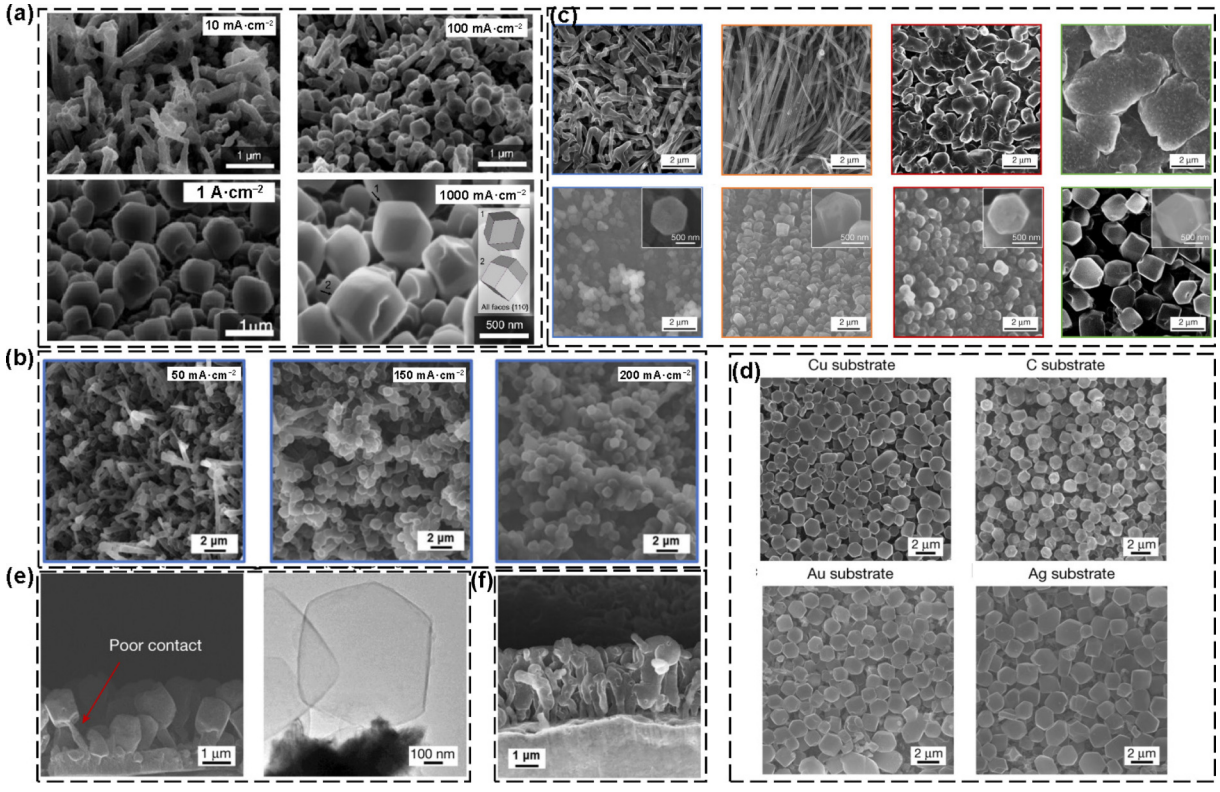

Figure 7 Current density affects the Li-current collector interface. (a) SEM images of lithium deposited at current densities of 10, 100, and 1000 mA·cm^{-2}. Reproduced with permission from Ref. [179], © American Chemical Society 2022. (b) SEM images of lithium deposited at current densities of 50, 150, and 200 mA·cm^{-2}.100 (c) Deposition morphology of lithium in various types of electrolytes at current densities of 1 mA·cm^{-2} (top) and 1000 mA·cm^{-2} (bottom) (from left to right, electrolytes are as follows: Electrolyte A: 1 M $LiPF_6$ in 1:1 v/v EC/DEC, Electrolyte B: 1 M $LiPF_6$ in PC with 2 wt.% $LiAsF_6$ and 2 wt.% FEC, Electrolyte C: 0.6 M LiDFOB and 0.6 M $LiBF_4$ in 1:1 v/v FEC/DEC, Electrolyte D: 4 M LiFSI in DME. At a current density of 1 mA·cm^{-2}, the deposition morphologies from left to right are filamentous, rod, columnar, and blocky, respectively; when the current density increases to 1000 mA·cm^{-2}, all morphologies become polyhedral). (d) Deposition morphology of lithium on different types of substrates (current density: 50 mA·cm^{-2}). (e) SEM (left) and cryogenic electron microscopy (right) cross-sectional views of rhombohedral dodecahedral lithium deposition in contact with the current collector. (f) SEM image of the cross-section of columnar lithium deposition in contact with the current collector. Reproduced with permission from Ref. [100], © Yuan, X. T. et al. 2023.

current density increased to 1000 mA·cm^{-2}, the deposition morphology of lithium in different types of electrolytes was polyhedral. Additionally, as depicted in Fig. 7(d), they also discovered that both non-lithiophilic (such as Cu, C) and lithiophilic (such as Au, Ag) substrates exhibit a rhombohedral dodecahedral deposition morphology under high current density (50 mA·cm^{-2}). However, the electrical connection between the rhombohedral dodecahedron lithium and the current collector is very poor, almost point contact, as shown in Fig. 7(e). This fragile Li-current collector interface easily leads to disconnection between lithium and the current collector, forming dead lithium. In contrast, the columnar lithium deposition at low current density (1 mA·cm^{-2}) has better electrical contact with the current collector (Fig. 7(f)). Due to the poor electrical connection between the rhombohedral dodecahedron and the current collector, a large amount of residual lithium is difficult to strip during the stripping process, and the lithium particles exhibit a contracted structure after partial dissolution, leading to an increase in dead lithium and a decrease in Coulombic efficiency. Although high current density leads to fragile connections between lithium and the current collector, appropriate application of high current density can achieve good contact. Yuan et al. found that using a high initial pulse current density (current density: 50 mA·cm^{-2}, capacity: 0.05 mAh·cm^{-2}) followed by a normal current density (current density: 1 mA·cm^{-2}, capacity: 0.95 mAh·cm^{-2}) achieves a denser deposition morphology than continuously using 1 mA·cm^{-2} to deposit 1 mAh·cm^{-2} capacity of lithium. This is because the initial pulse of high current density promotes tight nucleation of lithium in a short period [100, 180].

In summary, as the current density increases, the morphology of lithium deposition gradually transforms into a polyhedral structure, and when the current density exceeds a certain threshold, the deposition morphology is no longer influenced by the electrolyte and current collector substrate. However, the polyhedral structure of lithium has point contacts with the current collector, leading to a fragile Li-current collector interface that can be improved by using pulse current.

2.4 Stacking pressure

Applying stacking pressure on batteries has been proven to be an effective method for regulating the morphology of lithium deposition, achieving higher Coulombic efficiency, and extending cycle life [181–183]. As shown in Fig. 8(a), elongated lithium deposits with significant curvature can easily lose electrical connection with the current collector, leading to a large amount of unreacted lithium being encapsulated by an electrically insulating SEI, thereby forming dead lithium. Therefore, controlling the morphology of lithium deposition, as illustrated in Figs. 8(b) and 8(c), by gradually reducing the curvature of lithium deposits to form larger deposits can establish a stable Li-current collector interface. This ensures that lithium always maintains good electrical contact with the current collector before stripping, enhancing the reversibility of deposition/stripping. The ideal deposition morphology should be micro-pillar-shaped, with minimal curvature, large deposits, and a uniform SEI, as shown in Fig. 8(c), which facilitates the complete dissolution of lithium [101].

By applying stacking pressure, the transformation from Fig. 8(a) to Fig. 8(c) can be achieved. Fang et al. noted that applying stacking pressure promotes the morphology of lithium deposition towards collapse on the current collector, improving the electrical connection between lithium and the current collector [101], and

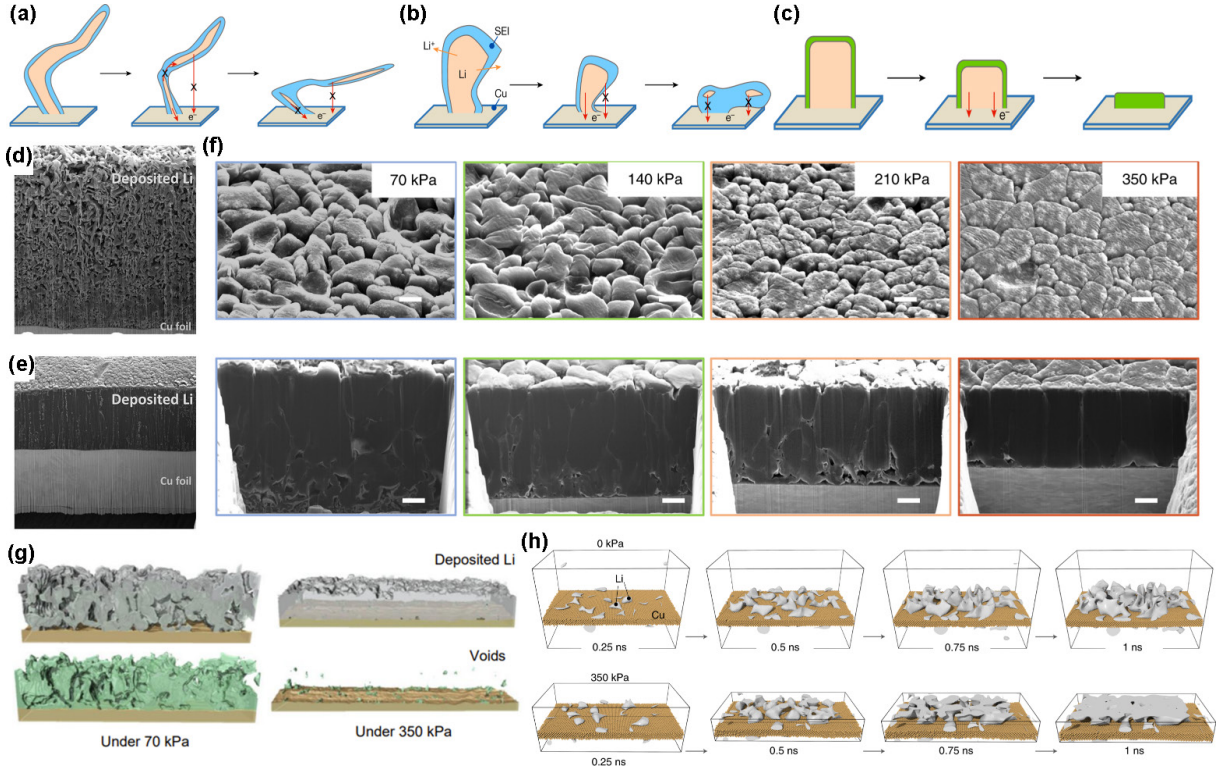

Figure 8 The impact of stacking pressure on the Li-current collector interface. (a)–(c) Schematics showing that the lower the tortuosity and the larger the bulk of lithium deposition, the better the electrical contact with the current collector, thus reducing the likelihood of dead lithium formation. Reproduced with permission from Ref. [101], © Fang, C. C. et al. 2019. (d) SEM images of lithium deposited on copper foil without applied pressure and (e) with an applied pressure of 1200 kPa. Reproduced with permission from Ref. [186], © American Chemical Society, 2023. (f) Top view (top) and cross-sectional view (bottom) of lithium deposited under stacking pressures of 70, 140, 210, and 350 kPa (current density: 2 mA·cm^{-2}, capacity: 2 mAh·cm^{-2}). (g) Three-dimensional images of lithium deposition and voids reconstructed from cryo-FIB-SEM image sequences. (The left side is under a stacking pressure of 70 kPa and the right side is under 350 kPa of stacking pressure; grey represents lithium and green represents voids). (h) Analysis of the impact of stacking pressure on lithium nucleation and early growth based on molecular dynamics simulations. Reproduced with permission from Ref. [187], © Fang, C. C. et al. 2021.

enhancing the battery's cycling performance [184, 185]. Kim et al. characterized the morphology of lithium deposition before and after applying stacking pressure, as shown in Fig. 8(d). Without stacking pressure, lithium deposits on the copper foil in a loose, elongated, and intertwined noodle-like manner with many holes and a thicker deposition. Under the same conditions but applying 1200 kPa pressure, as shown in Fig. 8(e), lithium deposits densely on the copper foil, displaying a good Li-current collector interface [186]. Fang et al. further investigated the role of stacking pressure [187]. As shown in Fig. 8(f), increasing the pressure from 70 to 350 kPa made the lithium deposition morphology increasingly dense, and the thickness significantly thinner. Especially when the stacking pressure reached 350 kPa, lithium exhibited a perfect columnar structure. The cross-sectional view reveals that under a lower stacking pressure, the lithium deposition layer above may connect tightly with each other, but significant holes exist at the bottom, especially near the contact with the current collector. These holes gradually disappear as the stacking pressure increases, indicating that stacking pressure significantly affects the initial stages of lithium nucleation and growth. They further reconstructed the three-dimensional image of lithium deposition under 70 and 350 kPa stacking pressure using cryo-focused ion beam (FIB)-SEM, as shown in Fig. 8(g), revealing poor contact between Li and the current collector under 70 kPa, especially with many gaps near the current collector. However, when the stacking pressure increased to 350 kPa, the contact between Li and the current collector was good, significantly reducing the porosity. This method also provides a reference for subsequent quantitative studies on the Li-current collector interface. They attempted to explain how stacking pressure affects the early stages of lithium nucleation and growth based on molecular dynamics. As shown in Fig. 8(h), without stacking pressure, Li nucleates randomly and grows uncontrollably, eventually forming elongated, uneven, porous deposits with poor electrical connection with the current collector. Under 350 kPa stacking pressure, the pressure promotes the connectivity of lithium nucleation sites and lateral growth during the growth process, eliminating voids during deposition and leading to uniform and dense lithium deposition.

In summary, applying stacking pressure (such as 350 kPa) can transform loose, elongated lithium deposition into a dense, bulk deposition morphology, resulting in a better Li-current collector interface [188, 189].

2.5 SEI

The SEI profoundly impacts battery performance, which includes the Li-current collector interface. SEI affects the lithium stripping process and can lead to the disconnection between lithium and the current collector during stripping, which results in the formation of dead lithium [3, 190]. As shown in Figs. 9(a)–9(f), the deposited lithium has good contact with the current collector and appears well-shaped at the beginning, but it gradually shrinks and becomes completely enveloped by the SEI during stripping. Eventually, it loses connection with the current collector and forms dead lithium. The EIS characterization, shown in Fig. 9(g), indicates that the interface resistance increases, and the lithium-ion diffusion coefficient decreases progressively throughout the stripping process. Hence, the stripping process can be summarized by the schematic shown in Fig. 9(h), which suggests that the SEI leads to a significant disconnection between lithium and the current collector during lithium stripping [191]. Lin et al.

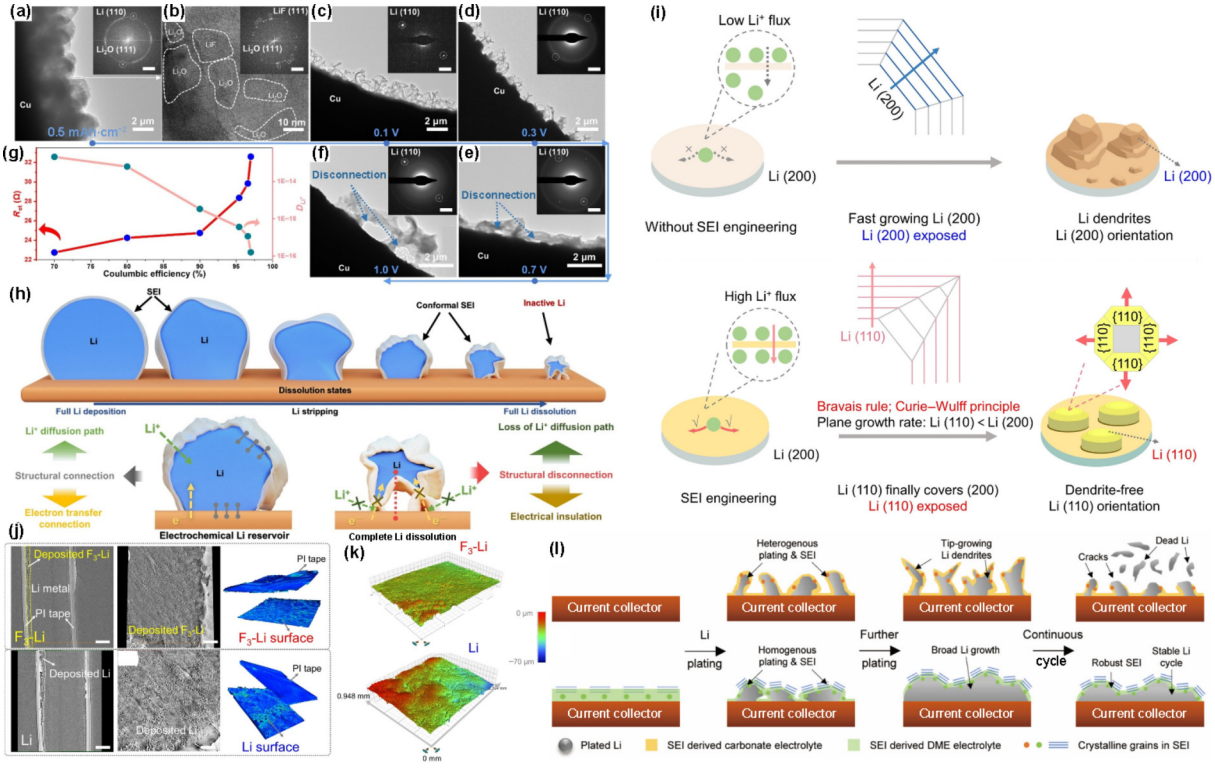

Figure 9 The SEI impacts the Li-current collector interface. Cryogenic electron microscopy images of (a) and (b) lithium deposited on a copper current collector at 0.5 mAh·cm^{-2} and the (c)–(f) subsequent stripping process. (g) Changes in interfacial impedance and lithium ion diffusion coefficients characterized by SEI during the stripping process. (h) Schematic illustration of lithium losing contact with the current collector during the stripping process. Reproduced with permission from Ref. [191], © Wiley-VCH GmbH 2024. (i) Schematic illustrations of conventional SEI inducing vertical Li (200) orientation deposition (top) versus SEI facilitating high Li^+ transport inducing planar Li (110) orientation deposition (bottom). (j) Side, left, and three-dimensional reconstruction views (from left to right) of lithium deposition characterized by CT for conventional SEI (bottom) versus SEI facilitating high Li^+ transport (top) (current density: 1 mA·cm^{-2}, capacity: 5 mAh·cm^{-2}). (k) White light microscopy characterization (capacity: 10 mAh·cm^{-2}). Reproduced with permission from Ref. [194], © Wiley-VCH GmbH 2023. (l) Schematic illustrations of lithium deposition under traditional SEI layer (top) versus SEI enriched with inorganic components (bottom). Reproduced with permission from Ref. [196], © Wi, T.-U. et al. 2023.

attempted to mitigate this issue by reserving an adequate amount of lithium to maintain contact between lithium and the current collector, ensuring the continuity of electron conduction paths and minimizing the formation of dead lithium [191].

Additionally, the SEI impacts the lithium deposition process, where the SEI's chemical composition, uniformity, and mechanical properties collectively determine the kinetics of lithium nucleation and initial growth [192, 193]. For instance, the SEI can induce lithium deposition along different crystal orientations. Since lithium atoms have a lower migration potential on the Li (110) plane compared to the Li (200) plane, lithium atoms diffusing along the Li (110) plane are prone to form planar, well-connected with current collector, dendrite-free lithium deposition morphologies. Conventional SEIs that facilitate slow and uneven lithium ion transport tend to induce vertical deposition oriented towards the Li (200) direction. Sun et al. designed a high-throughput SEI with high contents of LiF and $-Si(CH_3)_3$, which accelerates the transport kinetics of Li^+ ions, ensuring high concentrations of Li^+ ions beneath the SEI to promote planar-oriented Li (110) deposition, as illustrated in Fig. 9(i) [194]. They reconstructed the 3D morphology of lithium deposition using CT and observed the morphology of lithium deposition using microscopy, finding that the deposition morphology of lithium under the modified SEI was flatter, as shown in Fig. 9(j) and Fig. 9(k). Furthermore, lithium ions exhibit different conductivity properties in different SEI components, which also affects the Li-current collector interface [195]. The lithium flux imbalance caused by SEIs formed in conventional ester-based electrolyte systems leads to uneven lithium deposition, resulting in direct disconnection between lithium and the current collector. Wi et al. constructed an inorganic-rich SEI to evenly regulate lithium ion diffusion, achieving uniform and stable lithium deposition on the current collector, as shown in Fig. 9(l) [196].

In summary, the SEI influences the processes of lithium stripping and deposition. During stripping, lithium gradually shrinks and becomes fully enclosed by the SEI, losing connection with the current collector and forming dead lithium. Maintaining a clear electronic conduction path through methods such as reserving lithium can improve this situation. The chemical composition and uniformity of the SEI also affect the deposition process. For example, the slow and uneven lithium ion transport through a common SEI induces vertical lithium growth. Thus, designing SEIs with high lithium ion transport kinetics can achieve a better Li-current collector interface.

2.6 Electric field

The impact of the electric field on the Li-current collector interface is quite common. For example, during the manufacturing process of current collectors, it is inevitable to produce microstructures with high curvature radii, such as burrs, which can lead to the "tip effect", generating high electric fields around these points. This condition encourages lithium to preferentially nucleate and grow rapidly at these locations. The distribution of the electric field within the battery is strongly related to the shape of the current collector, thus the strategies discussed in Section 2.1.4 for altering the topological structure of the current collector and constructing 3D current collectors can also be analyzed from the perspective of electric field regulation and its impact on the Li-current collector interface [197]. After constructing a 3D current collector with a porous structure, a large number of microstructures with high curvature radii will appear within the 3D structure of the current collector, inducing lithium to deposit internally and thereby suppressing the formation of lithium dendrites [139]. Additionally, the internal electric field generated during the charging and discharging process of the battery can also serve as a strategy for improving the Li-current collector interface. For instance, Liu et al. found that dead lithium highly responds to the electric field generated during battery operation [198]. As illustrated in Fig. 10(a), an electric field from the positive to the negative electrode is generated inside the battery during charging, inducing an opposite electric field within the dead lithium. This leads to a negative overpotential at the end of the dead lithium closer to the positive electrode, causing lithium deposition at this

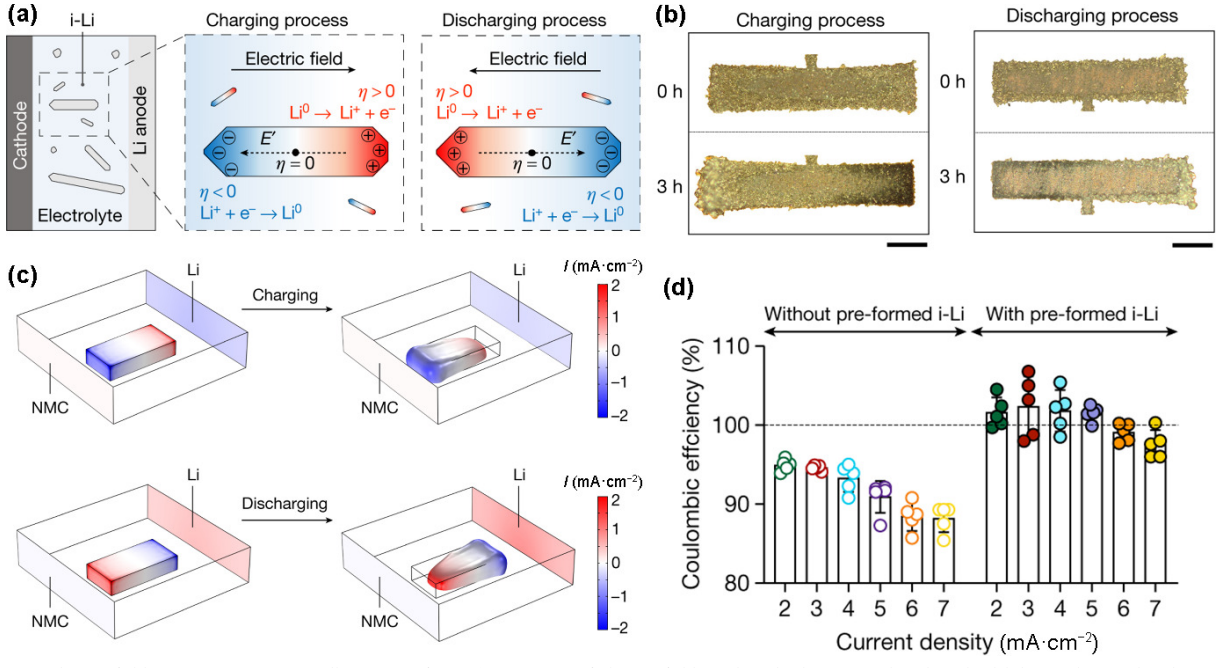

Figure 10 Electric field impacts Li-current collector interface. (a) Direction of electric fields within the battery and within dead lithium during the charging and discharging process, along with the accumulation of charges in dead lithium. Blue and red represent negative and positive charges, respectively. (b) Optical images of a lithium island at the beginning (t = 0 h) and an intermediate state (t = 3 h) during the charging and discharging process (scale = 100 μm). (c) Current density of a lithium island at the initial state (t = 100 s) and an intermediate state (t = 2 h) during the charging and discharging process. (d) Coulombic efficiency of batteries with and without dead lithium at different current densities. Reproduced with permission from Ref. [198], © Liu, F. et al. 2021.

end. Conversely, the end closer to the negative electrode exhibits a positive overpotential, leading to lithium dissolution. The reverse occurs during the discharge process. Experimental and simulation results also confirmed the above analysis. As shown in Figs. 10(b) and 10(c), during the charging process, dead lithium islands in the battery dissolve on the side closer to the negative electrode (right end) and deposit new lithium on the side closer to the positive electrode (left end). The discharge process is opposite. Therefore, this approach holds the promise of moving the dead lithium in the battery that has lost contact with the current collector towards the negative electrode during the discharge process, achieving recontact with the current collector. As shown in Fig. 10(d), Coulombic efficiency measurements also indicate that the efficiency of a battery configured with dead lithium can even exceed 100%, proving that utilizing the electric field can revive dead lithium and enhance efficiency.

In summary, electric fields have an impact on lithium deposition. For example, small structures on the current collector, such as burrs or irregularities, create high electric field intensities due to the tip effect, leading to preferential nucleation and rapid growth of lithium at these sites. This phenomenon is more pronounced when constructing current collectors with three-dimensional structures. Additionally, during the charging and discharging processes, the electric field within the battery can induce an internal electric field within the lithium. This internal field generates a potential difference across the ends of the lithium, causing one end to dissolve while the other grows, which could potentially reconnect "dead" lithium to the current collector. However, the current understanding of the impact of the electric field on the Li-current collector interface is limited, and research in this area is sparse. For instance, the solid–solid interface between lithium and the current collector, as well as the solid–liquid interface between the electrolyte and the electrode, can cause abrupt changes in the electric field; the deposition of lithium continuously alters the internal electric field of the battery, which further affects lithium deposition; the accumulation of surface charges on the SEI during battery operation can also cause local electric field distortions. These variations in the electric field will profoundly influence the lithium deposition process and affect the Li-current collector interface. Therefore, both the mechanism by which the electric field influences the Li-current collector interface and the use of electric fields to enhance performance merit more in-depth research in the future.

2.7 Temperature

In practical applications, batteries are required to operate under various environmental temperatures, which impacts their performance, including the Li-current collector interface [199, 200]. For example, at low temperatures, slow lithium ion transport near the anode can lead to uneven lithium deposition [201]. As shown in Fig. 11(a), Tao et al. observed the morphology of lithium deposition at 0, 25, and 50 °C, respectively [202]. At 0 °C, the morphology of lithium deposition is uneven, with both dark and light areas. The light areas show dendritic deposition, while the dark areas are blocky deposits. As the temperature increases to 25 °C, the proportion of dendritic deposition areas decreases. At 50 °C, the light deposition areas further shrink, no longer showing dendritic deposition but instead blocky deposition. The deposition morphology in the dark areas appears dense, compact, and flat. Using SEM combined with *in situ* nuclear magnetic resonance (NMR), they illustrated the deposition process of lithium at different temperatures, as shown in Fig. 11(b). At 0 and 25 °C, a similar growth pattern of lithium is observed: it starts with dendritic formation and, as deposition progresses, gradually develops into blocky lithium laterally, only to revert back to dendritic lithium during the stripping process. At 50 °C, lithium initially grows as dendritic but later, lateral deposition dominates, gradually forming a dense deposition morphology. Further, through simulation, they modeled the thermal and electric field distribution at 0 and 50 °C. As illustrated in Figs. 11(c) and 11(d), at 0 °C, there is a significant temperature gradient from the tip to the base of the lithium deposition, but at 50 °C, the thermal field distribution is more uniform. Additionally, as shown in Figs. 11(e) and 11(f), the electric field distribution at 0 °C is more uneven compared to 50 °C, making it difficult to achieve dense and uniform deposition as at 50 °C.

In summary, it has been found that low temperatures are conducive to the formation of dendritic lithium, while increasing the temperature can promote lateral growth of lithium and form a flatter deposition morphology. However, the understanding of the impact of temperature on the Li-current collector interface is still insufficient. For example, the thermal properties of lithium and the current collector (such as copper) differ greatly, with the linear thermal expansion coefficient of copper (4.6×10^{-5} °C^{-1}) being almost three times that of lithium (1.65×10^{-5} °C^{-1}). Therefore, stress may occur at the interface during temperature changes. Additionally, the thermal conductivity of lithium (85 W·m^{-1}·K^{-1}), copper (401 W·m^{-1}·K^{-1}), and the electrolyte (usually less than 1 W·m^{-1}·K^{-1}) varies significantly, and the presence of interface thermal resistance results in severely uneven heat distribution among the components. Thus, further research is needed on the impact of temperature on the Li-current collector interface.

3 Conclusion and outlook

This review summarizes the latest research advancements on the

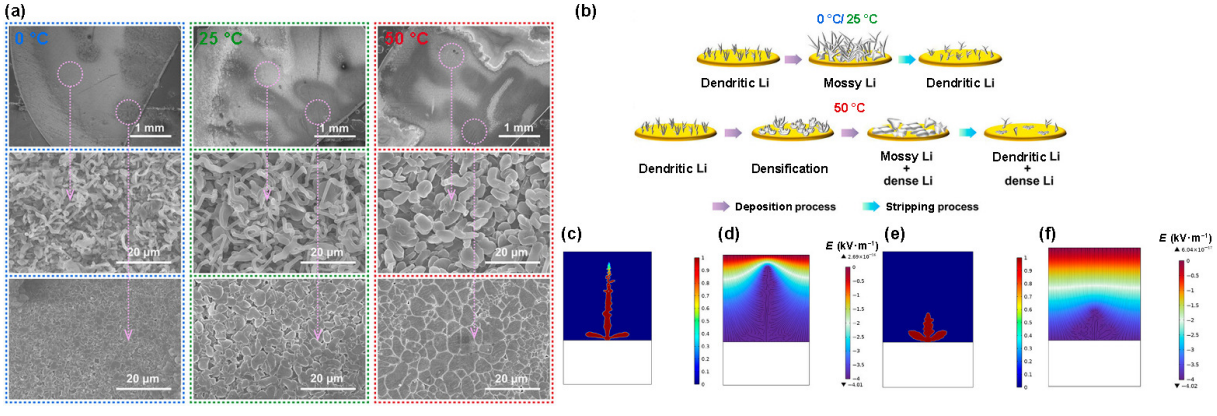

Figure 11 Temperature impacts the Li-current collector interface. (a) Morphology of lithium deposition at 0, 25, and 50 °C (from left to right). (b) Schematic illustrations of changes in lithium deposition morphology at 0, 25, and 50 °C. At 0 °C, (c) temperature field and (d) electric field distribution, and at 50 °C, (e) temperature field and (f) electric field distribution. Reproduced with permission from Ref. [202], © American Chemical Society 2023.

solid–solid interface between lithium metal and current collectors, drawing several key conclusions:

(1) The properties of current collector substrates profoundly influence the Li-current collector interface. Introducing lithiophilic sites, altering the crystal facets of current collectors, utilizing soft substrates, and constructing three-dimensional collectors with small pore sizes, large pore volumes, and high electroactive surface area ratios are promising approaches for optimizing the Li-current collector interface.

(2) Electrolyte chemistry also impacts the Li-current collector interface. Utilizing electrolytes with appropriate solvent strength and concentration, altering electrolyte composition, and using additives can improve the interface.

(3) The current density influences the morphology of lithium deposition. A higher current density tends to favor the deposition of lithium in a polyhedral structure, leading to a fragile Li-current collector interface.

(4) Appropriately applying stacking pressure can result in a better deposition morphology of lithium, thereby enhancing the interface.

(5) The chemical composition, uniformity, and mechanical properties of the SEI all impact the deposition and stripping processes of lithium, leading to disconnection between lithium and the current collector. Therefore, regulating the SEI is an effective method to enhance the Li-current collector interface.

(6) Electric fields influence lithium deposition and growth, thus, utilizing electric fields to induce dense lithium deposition and reconnect dead lithium with the current collector can achieve a superior interface.

(7) Temperature changes affect the deposition process of lithium. Low temperatures are detrimental to the formation of a good Li-current collector interface.

In summary, many factors can influence the Li-current collector interface. Identifying and thoroughly researching the most significant factor to achieve a stable and optimal Li-current collector interface is crucial. Unfortunately, the current research on the Li-current collector interface, as shown in existing findings, remains qualitative and lacks quantitative analysis. This qualitative approach means that different studies' results are difficult to directly compare due to the absence of standardized quantitative benchmarks. However, this also indicates that our current understanding is still superficial, presenting numerous opportunities for future research. As shown in Fig. 12, potential directions for future studies might include:

(1) First and foremost is developing quantitative characterization methods for the Li-current collector interface. Current research largely relies on qualitative observations using SEM, TEM, and similar methods to view lithium deposition on current collectors, lacking quantitative characterization of the contact area and bonding strength between lithium and the collector. Some studies have used CT and similar methods to achieve high-resolution 3D structures of lithium deposition, further obtaining maps of porosity distribution and changes in the height of lithium deposition [114, 135, 187]. Therefore, this

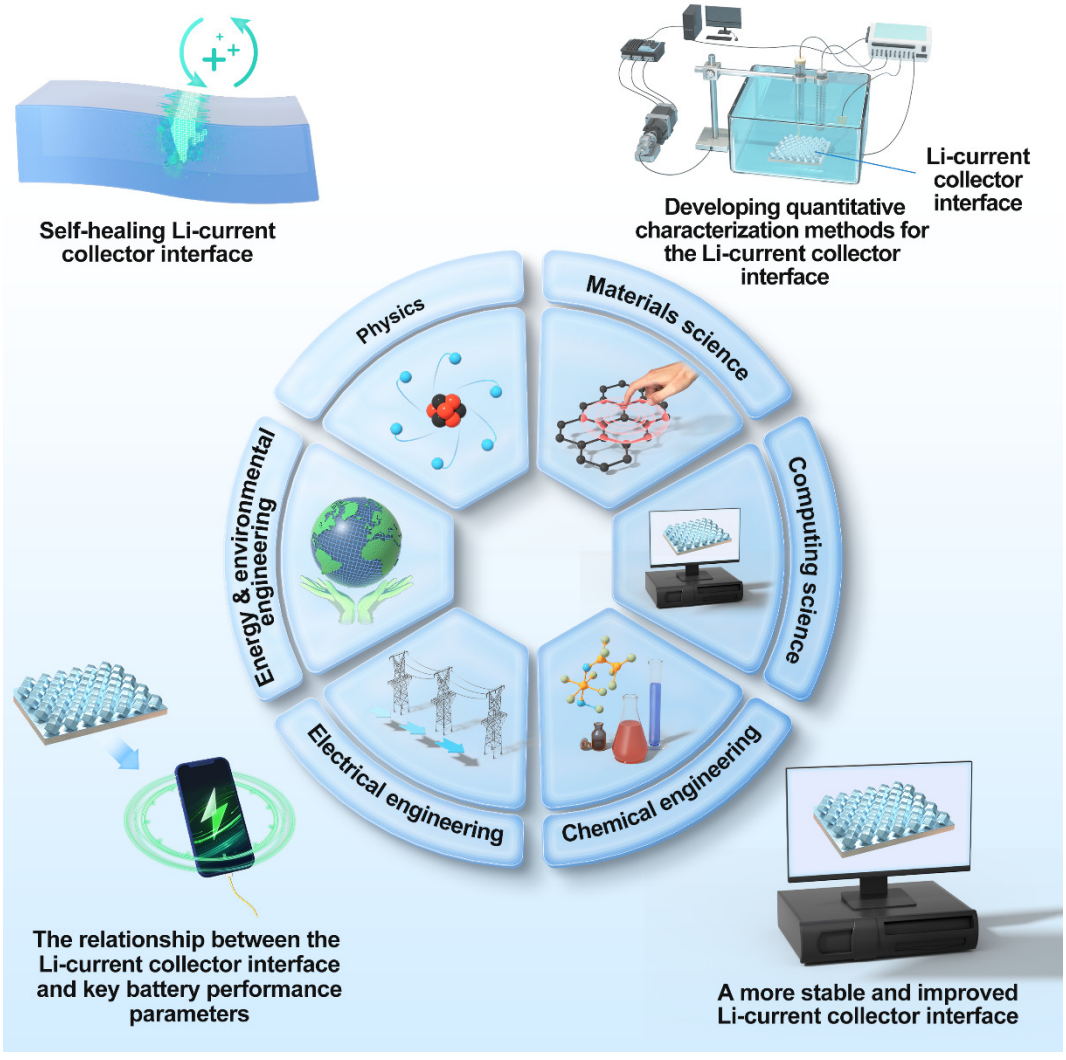

Figure 12 Future development directions for Li-current collector interface research.

method has the potential to serve as quantitative characterization schemes for the contact area between lithium and the current collector. Additionally, characterizing physical parameters that change with the Li-current collector interface to indirectly reflect its variation, including electrical, thermal, and mechanical parameters, is also worth considering. For instance, changes in the contact situation between lithium and the collector could lead to overall changes in electrical conductivity, suggesting that quantitative measurements of such changes could reflect interface variations. Changes in the Li-current collector interface could also alter contact resistance, affecting Joule heating when current passes through, which could be mapped using infrared thermography and recently reported non-destructive methods like X-ray diffraction computed tomography (XRD-CT) [203]. Moreover, establishing uniform standards for characterization is crucial, facilitating direct comparisons between different studies.

(2) How to obtain a more stable and improved Li-current collector interface still requires further investigation. Although this review has summarized some strategies to improve the Li-current collector interface based on existing literature, there is still a lack of direct and quantitative research. Therefore, developing or adopting new research and characterization methods is becoming essential to overcome this bottleneck issue. For example, with the rapid advancement of computational science in recent years, technologies such as machine learning and materials computation have been widely applied in scientific research. Using computational methods for high-throughput screening could potentially identify material systems that form a robust Li-current collector interface. Additionally, these methods could analyze experimental phenomena to predict more effective material modification strategies. Another example is the development of new *in situ* characterization techniques, especially for *in situ* electrical parameter characterization (such as local current and conductivity), which is crucial for deeply understanding the interface characteristics within batteries, including the Li-current collector interface. These parameters are directly related to the migration of electrons and ions. Currently, there is a lack of research in this area, and the few existing results only provide overall electrical parameters of the interface. In summary, developing and applying new research methods to achieve a stable and improved Li-current collector interface is vital.

(3) The relationship function between the Li-current collector interface and key battery performance parameters still requires further investigation. How a stable and optimal Li-current collector interface can better contribute to high-performance batteries, ensuring longer cycle life and higher Coulombic efficiency, also warrants further attention.

(4) Self-healing intelligent Li-current collector interfaces may become an exciting research topic in the future. In recent years, intelligent materials and smart devices have garnered increasing attention. Materials degrade and develop defects over time, shortening their lifespan or causing sudden failures. Hence, intelligent materials that can self-heal, much like animals recovering from injuries, have become a focal point. Capturing physical signals of defects and incorporating materials capable of eliminating these defects into the matrix is currently an effective approach to achieving this concept. For example, in the field of electrical insulation, self-healing polymer dielectrics capable of repairing electrical damage have been developed [203]. By incorporating superparamagnetic nanoparticles into polymer dielectrics, the magnetocaloric effect induced by electric damage can cause these nanoparticles to migrate to the defect site and repair it. Similarly, the Li-current collector interface can develop defects during repeated cycling, which can degrade its initially good performance. Therefore, incorporating additives into the electrolyte to detect and timely eliminate these defects could be a novel and intriguing approach to enhance battery performance.

In summary, constructing a stable and good solid–solid interface between lithium and the current collector is crucial for high-performance LMBs, and the exploration of this topic is currently in a booming phase. Addressing the fragile Li-current collector interface issue requires interdisciplinary collaboration across chemical engineering, material science, electrical engineering, computational science, physics, energy and environmental engineering. With the rapid development of LMBs bringing opportunities, along with the swift progress in analytical characterization techniques, machine learning, and theoretical computations, we look forward to the proposal of better strategies for achieving an improved Li-current collector interface, ensuring this challenge no longer remains a bottleneck for the advancement of high-performance LMBs.

Acknowledgements

We acknowledge the support of the National Science Foundation (No. CBET-2143677).

References

[1] Li, M.; Lu, J.; Chen, Z. W.; Amine, K. 30 years of lithium-ion batteries. *Adv. Mater.* **2018**, *30*, 1800561.

[2] Deng, J.; Bae, C.; Denlinger, A.; Miller, T. Electric vehicles batteries: Requirements and challenges. *Joule* **2020**, *4*, 511–515.

[3] Zhou, B. X.; Bonakdarpour, A.; Stoševski, I.; Fang, B. Z.; Wilkinson, D. P. Modification of Cu current collectors for lithium metal batteries—A review. *Prog. Mater. Sci.* **2022**, *130*, 100996.

[4] Wang, T.-Y.; Mao, J.; Zhang, B. Y.; Zhang, G.-X.; Dang, Z.-M. Polymeric insulating materials characteristics for high-voltage applications. *Nat. Rev. Electr. Eng.*, in press, DOI: 10.1038/s44287-024-00070-5.

[5] Liu, G. X.; Wan, W.; Nie, Q.; Zhang, C.; Chen, X. L.; Lin, W. H.; Wei, X. Z.; Huang, Y. H.; Li, J.; Wang, C. Controllable long-term lithium replenishment for enhancing energy density and cycle life of lithium-ion batteries. *Energy Environ. Sci.* **2024**, *17*, 1163–1174.

[6] Wang, Y. Q.; Wu, Z. Z.; Azad, F. M.; Zhu, Y. T.; Wang, L. Z.; Hawker, C. J.; Whittaker, A. K.; Forsyth, M.; Zhang, C. Fluorination in advanced battery design. *Nat. Rev. Mater.* **2023**, *9*, 119–133.

[7] Pacala, S.; Socolow, R. Stabilization wedges: Solving the climate problem for the next 50 years with current technologies. *Science* **2004**, *305*, 968–972.

[8] Goodenough, J. B.; Kim, Y. Challenges for rechargeable Li batteries. *Chem. Mater.* **2010**, *22*, 587–603.

[9] Tarascon, J. M.; Armand, M. Issues and challenges facing rechargeable lithium batteries. *Nature* **2001**, *414*, 359–367.

[10] Go, W.; Kim, M. H.; Park, J.; Lim, C. H.; Joo, S. H.; Kim, Y.; Lee, H. W. Nanocrevasse-rich carbon fibers for stable lithium and sodium metal anodes. *Nano Lett.* **2019**, *19*, 1504–1511.

[11] Zhu, P. C.; Gastol, D.; Marshall, J.; Sommerville, R.; Goodship, V.; Kendrick, E. A review of current collectors for lithium-ion batteries. *J. Power Sources* **2021**, *485*, 229321.

[12] Xu, K. Nonaqueous liquid electrolytes for lithium-based rechargeable batteries. *Chem. Rev.* **2004**, *104*, 4303–4418.

[13] Huang, X. S. Separator technologies for lithium-ion batteries. *J. Solid State Electrochem.* **2011**, *15*, 649–662.

[14] Zuo, L. L.; Ma, Q.; Xiao, P. T.; Guo, Q. P.; Xie, W.; Lu, D.; Yun, X.; Zheng, C.; Chen, Y. Upgrading the separators integrated with desolvation and selective deposition toward the stable lithium metal batteries. *Adv. Mater.* **2024**, *36*, 2311529.

[15] Ding, L. Y.; Yue, X. Y.; Zhang, X. H.; Chen, Y. M.; Liu, J. J.; Shi, Z. Q.; Wang, Z. Y.; Yan, X. Z.; Liang, Z. A polyimine aerogel separator with electron cloud design to boost Li-ion transport for stable Li metal batteries. *Proc. Natl. Acad. Sci. USA* **2023**, *120*, e2314264120.

[16] Zhu, P. C.; Driscoll, E. H.; Dong, B.; Sommerville, R.; Zorin, A.; Slater, P. R.; Kendrick, E. Direct reuse of aluminium and copper current collectors from spent lithium-ion batteries. *Green Chem.* **2023**, *25*, 3503–3514.
[17] Wen, Z. X.; Fang, W. Q.; Wang, F. L.; Kang, H.; Zhao, S. Q.; Guo, S. J.; Chen, G. Dual-salt electrolyte additive enables high moisture tolerance and favorable electric double layer for lithium metal battery. *Angew. Chem., Int. Ed.* **2024**, *63*, e202314876.
[18] Kang, Q.; Li, Y.; Zhuang, Z. C.; Yang, H. J.; Luo, L. X.; Xu, J.; Wang, J.; Guan, Q. H.; Zhu, H.; Zuo, Y. Z. et al. Engineering a dynamic solvent-phobic liquid electrolyte interphase for long-life lithium metal batteries. *Adv. Mater.* **2024**, *36*, 2308799.
[19] Wu, K.; Ran, P. L.; Wang, B. T.; Wang, F. W.; Zhao, J. K.; Zhao, E. Y. Diffusion-optimized long lifespan 4.6 V $LiCoO_2$: Homogenizing cycled bulk-to-surface Li concentration with reduced structure stress. *Adv. Sci.* **2024**, *11*, 2308258.
[20] Lin, C.; Li, J. Y.; Yin, Z. W.; Huang, W. Y.; Zhao, Q. H.; Weng, Q. S.; Liu, Q.; Sun, J. L.; Chen, G. H.; Pan, F. Structural understanding for high-voltage stabilization of lithium cobalt oxide. *Adv. Mater.* **2024**, *36*, 2307404.
[21] Kim, S.; Lee, J. A.; Lee, D. G.; Son, J.; Bae, T. H.; Lee, T. K.; Choi, N. S. Designing electrolytes for stable operation of high-voltage $LiCoO_2$ in lithium-ion batteries. *ACS Energy Lett.* **2024**, *9*, 262–270.
[22] Chen, W. X.; Muhtar, D.; Li, K. L.; Xiao, G. F.; Cao, J.; Tang, Y. Y.; Qian, G. Y.; Lu, X. Y.; Sun, Y.; Lu, X. Regulating cation disorder triggered-electronic reshuffling for sustainable conventional layered oxide cathodes. *Chem. Mater.* **2024**, *36*, 1249–1261.
[23] Qin, Z. Y.; Zhang, T.; Gao, X. S.; Luo, W. Q.; Han, J. W.; Lu, B. G.; Zhou, J.; Chen, G. Self-reconstruction of highly degraded $LiNi_{0.8}Co_{0.1}Mn_{0.1}O_2$ toward stable single-crystalline cathode. *Adv. Mater.* **2024**, *36*, 2307091.
[24] Wan, H. L.; Wang, Z. Y.; Zhang, W. R.; He, X. Z.; Wang, C. S. Interface design for all-solid-state lithium batteries. *Nature* **2023**, *623*, 739–744.
[25] Pandya, R.; Valzania, L.; Dorchies, F.; Xia, F.; Mc Hugh, J.; Mathieson, A.; Tan, H. J.; Parton, T. G.; Godeffroy, L.; Mazloomian, K. et al. Three-dimensional *operando* optical imaging of particle and electrolyte heterogeneities inside Li-ion batteries. *Nat. Nanotechnol.* **2023**, *18*, 1185–1194.
[26] Klein, S.; Van Wickeren, S.; Röser, S.; Bärmann, P.; Borzutzki, K.; Heidrich, B.; Börner, M.; Winter, M.; Placke, T.; Kasnatscheew, J. Understanding the outstanding high-voltage performance of NCM523||graphite lithium ion cells after elimination of ethylene carbonate solvent from conventional electrolyte. *Adv. Energy Mater.* **2021**, *11*, 2003738.
[27] Liu, C.; Li, F.; Ma, L. P.; Cheng, H. M. Advanced materials for energy storage. *Adv. Mater.* **2010**, *22*, E28–E62.
[28] Syed, M. A.; Salehabadi, M.; Obrovac, M. N. High energy density large particle $LiFePO_4$. *Chem. Mater.* **2024**, *36*, 803–814.
[29] Zhao, X. X.; Wang, X. T.; Guo, J. Z.; Gu, Z. Y.; Cao, J. M.; Yang, J. L.; Lu, F. Q.; Zhang, J. P.; Wu, X. L. Dynamic Li^+ capture through ligand-chain interaction for the regeneration of depleted $LiFePO_4$ cathode. *Adv. Mater.* **2024**, *36*, 2308927.
[30] Ding, J.; Hu, W. B.; Paek, E.; Mitlin, D. Review of hybrid ion capacitors: From aqueous to lithium to sodium. *Chem. Rev.* **2018**, *118*, 6457–6498.
[31] Kim, M. H.; Kim, J.; Choi, S. H.; Wi, T. U.; Choi, A.; Seo, J.; Lim, C. H.; Park, C.; Lee, H. W. Mitigating electrode-level heterogeneity using phosphorus nanolayers on graphite for fast-charging batteries. *ACS Energy Lett.* **2023**, *8*, 3962–3970.
[32] Tu, S. B.; Zhang, B.; Zhang, Y.; Chen, Z. H.; Wang, X. C.; Zhan, R. M.; Ou, Y. T.; Wang, W. Y.; Liu, X. R.; Duan, X. R. et al. Fast-charging capability of graphite-based lithium-ion batteries enabled by Li_3P-based crystalline solid-electrolyte interphase. *Nat. Energy* **2023**, *8*, 1365–1374.
[33] Pendashteh, A.; Tomey, R.; Vilatela, J. J. Nanotextile 100% Si anodes for the next generation energy-dense Li-ion batteries. *Adv. Energy Mater.* **2024**, *14*, 2304018.
[34] Kim, N.; Kim, Y.; Sung, J.; Cho, J. Issues impeding the commercialization of laboratory innovations for energy-dense Si-containing lithium-ion batteries. *Nat. Energy* **2023**, *8*, 921–933.
[35] Yan, W. L.; Mu, Z. L.; Wang, Z. X.; Huang, Y. L.; Wu, D. X.; Lu, P. S.; Lu, J. Z.; Xu, J. R.; Wu, Y. J.; Ma, T. H. et al. Hard-carbon-stabilized Li–Si anodes for high-performance all-solid-state Li-ion batteries. *Nat. Energy* **2023**, *8*, 800–813.
[36] Vetter, J.; Novák, P.; Wagner, M. R.; Veit, C.; Möller, K. C.; Besenhard, J. O.; Winter, M.; Wohlfahrt-Mehrens, M.; Vogler, C.; Hammouche, A. Ageing mechanisms in lithium-ion batteries. *J. Power Sources* **2005**, *147*, 269–281.
[37] Endo, Y.; Yan, X.; Li, M.; Akiyama, R.; Brandl, C.; Liu, J. Z.; Hobara, R.; Hasegawa, S.; Wan, W. S.; Novoselov, K. S. et al. Dynamic topological domain walls driven by lithium intercalation in graphene. *Nat. Nanotechnol.* **2023**, *18*, 1154–1161.
[38] Jamnuch, S.; Pascal, T. A. Electronic signatures of Lorentzian dynamics and charge fluctuations in lithiated graphite structures. *Nat. Commun.* **2023**, *14*, 2291.
[39] Xiao, Y. H.; Wang, Y.; Bo, S. H.; Kim, J. C.; Miara, L. J.; Ceder, G. Understanding interface stability in solid-state batteries. *Nat. Rev. Mater.* **2019**, *5*, 105–126.
[40] Cheng, X. B.; Zhang, R.; Zhao, C. Z.; Zhang, Q. Toward safe lithium metal anode in rechargeable batteries: A review. *Chem. Rev.* **2017**, *117*, 10403–10473.
[41] Han, Y. Y.; Liu, B.; Xiao, Z.; Zhang, W. K.; Wang, X. L.; Pan, G. X.; Xia, Y.; Xia, X. H.; Tu, J. P. Interface issues of lithium metal anode for high-energy batteries: Challenges, strategies, and perspectives. *InfoMat* **2021**, *3*, 155–174.
[42] Rajagopalan, R.; Tang, Y. G.; Ji, X. B.; Jia, C. K.; Wang, H. Y. Advancements and challenges in potassium ion batteries: A comprehensive review. *Adv. Funct. Mater.* **2020**, *30*, 1909486.
[43] Albertus, P.; Babinec, S.; Litzelman, S.; Newman, A. Status and challenges in enabling the lithium metal electrode for high-energy and low-cost rechargeable batteries. *Nat. Energy* **2017**, *3*, 16–21.
[44] Lin, D. C.; Liu, Y. Y.; Cui, Y. Reviving the lithium metal anode for high-energy batteries. *Nat. Nanotechnol.* **2017**, *12*, 194–206.
[45] Xie, Y. X.; Huang, Y. X.; Chen, H.; Lin, W. R.; Wu, T. R.; Wang, Y. Q.; Liu, S. S.; Sun, M. L.; Huang, H. Y.; Dai, P. et al. Dual-protective role of PM475: Bolstering anode and cathode stability in lithium metal batteries. *Adv. Funct. Mater.* **2024**, *34*, 2310867.
[46] Kim, M. H.; Wi, T. U.; Seo, J.; Choi, A.; Ko, S.; Kim, J.; Jung, U.; Kim, M. S.; Park, C.; Jin, S. et al. Design principles for fluorinated interphase evolution via conversion-type alloying processes for anticorrosive lithium metal anodes. *Nano Lett.* **2023**, *23*, 3582–3591.
[47] Cao, J. Q.; Shi, Y. S.; Gao, A. S.; Du, G. Y.; Dilxat, M.; Zhang, Y. F.; Cai, M. H.; Qian, G. Y.; Lu, X. Y.; Xie, F. F. et al. Hierarchical Li electrochemistry using alloy-type anode for high-energy-density Li metal batteries. *Nat. Commun.* **2024**, *15*, 1354.
[48] Zhang, W. R.; Koverga, V.; Liu, S. F.; Zhou, J. G.; Wang, J.; Bai, P. X.; Tan, S.; Dandu, N. K.; Wang, Z. Y.; Chen, F. et al. Single-phase local-high-concentration solid polymer electrolytes for lithium-metal batteries. *Nat. Energy* **2024**, *9*, 386–400.
[49] Kim, J. T.; Su, H.; Zhong, Y.; Wang, C. Z.; Wu, H. Y.; Zhao, D. Y.; Wang, C. H.; Sun, X. L.; Li, Y. Z. All-solid-state lithium-sulfur batteries through a reaction engineering lens. *Nat. Chem. Eng.* **2024**, *1*, 400–410.
[50] Su, L. L.; Yao, N.; Li, Z.; Bi, C. X.; Chen, Z. X.; Chen, X.; Li, B. Q.; Zhang, X. Q.; Huang, J. Q. Improving rate performance of encapsulating lithium-polysulfide electrolytes for practical lithium-sulfur batteries. *Angew. Chem., Int. Ed.* **2024**, *63*, e202318785.
[51] Zhou, S. Y.; Shi, J.; Liu, S. G.; Li, G.; Pei, F.; Chen, Y. H.; Deng, J. X.; Zheng, Q. Z.; Li, J. Y.; Zhao, C. et al. Visualizing interfacial collective reaction behaviour of Li-S batteries. *Nature* **2023**, *621*, 75–81.
[52] Zhao, Z. Q.; Pan, Y. K.; Yi, S.; Su, Z.; Chen, H. L.; Huang, Y. N.; Niu, B.; Long, D. H.; Zhang, Y. Y. Enhanced electron delocalization within coherent nano-heterocrystal ensembles for optimizing polysulfide conversion in high-energy-density Li-S batteries. *Adv. Mater.* **2024**, *36*, 2310052.
[53] Ahn, S.; Zor, C.; Yang, S. X.; Lagnoni, M.; Dewar, D.; Nimmo, T.; Chau, C.; Jenkins, M.; Kibler, A. J.; Pateman, A. et al. Why

charging Li-air batteries with current low-voltage mediators is slow and singlet oxygen does not explain degradation. *Nat. Chem.* **2023**, *15*, 1022–1029.

[54] Tian, S. L.; Song, L. N.; Chang, L. M.; Liu, W. Q.; Wang, H. F.; Xu, J. J. A force-assisted Li-O_2 battery based on piezoelectric catalysis and band bending of MoS_2/Pd cathode. *Adv. Energy Mater.* **2024**, *14*, 2303215.

[55] Zhang, Y.; Zhang, S. T.; Li, H. N.; Lin, Y. R.; Yuan, M. W.; Nan, C. Y.; Chen, C. Tunable oxygen vacancies of cobalt oxides in lithium-oxygen batteries: Morphology control of discharge product. *Nano Lett.* **2023**, *23*, 9119–9125.

[56] Xie, Y. X.; Huang, Y. X.; Zhang, Y. G.; Wu, T. R.; Liu, S. S.; Sun, M. L.; Lee, B.; Lin, Z.; Chen, H.; Dai, P. et al. Surface modification using heptafluorobutyric acid to produce highly stable Li metal anodes. *Nat. Commun.* **2023**, *14*, 2883.

[57] Zou, Y. G.; Liu, G.; Wang, Y. Q.; Li, Q.; Ma, Z.; Yin, D. M.; Liang, Y.; Cao, Z.; Cavallo, L.; Kim, H. et al. Intermolecular interactions mediated nonflammable electrolyte for high-voltage lithium metal batteries in wide temperature. *Adv. Energy Mater.* **2023**, *13*, 2300443.

[58] Mao, M. L.; Ji, X.; Wang, Q. Y.; Lin, Z. J.; Li, M. Y.; Liu, T.; Wang, C. L.; Hu, Y. S.; Li, H.; Huang, X. J. et al. Anion-enrichment interface enables high-voltage anode-free lithium metal batteries. *Nat. Commun.* **2023**, *14*, 1082.

[59] Hobold, G. M.; Kim, K. H.; Gallant, B. M. Beneficial *vs*. inhibiting passivation by the native lithium solid electrolyte interphase revealed by electrochemical Li^+ exchange. *Energy Environ. Sci.* **2023**, *16*, 2247–2261.

[60] Zhang, S. H.; Sun, F.; Du, X. F.; Zhang, X. H.; Huang, L.; Ma, J.; Dong, S. M.; Hilger, A.; Manke, I.; Li, L. S. et al. *In situ*-polymerized lithium salt as a polymer electrolyte for high-safety lithium metal batteries. *Energy Environ. Sci.* **2023**, *16*, 2591–2602.

[61] Kim, S. C.; Oyakhire, S. T.; Athanitis, C.; Wang, J. Y.; Zhang, Z. W.; Zhang, W. B.; Boyle, D. T.; Kim, M. S.; Yu, Z. A.; Gao, X. et al. Data-driven electrolyte design for lithium metal anodes. *Proc. Natl. Acad. Sci. USA* **2023**, *120*, e2214357120.

[62] Cheng, Q.; Chen, Z. X.; Li, X. Y.; Bi, C. X.; Sun, F. R.; Zhang, X. Q.; Ma, X. Z.; Li, B. Q.; Huang, J. Q. Deciphering the degradation mechanism of high-rate and high-energy-density lithium-sulfur pouch cells. *Adv. Energy Mater.* **2023**, *13*, 2301770.

[63] Liang, H. M.; Wang, L.; Song, Y. Z.; Ren, D. S.; Wang, A. P.; Yang, Y.; Xu, H.; Sun, Y. M.; He, X. M. Manipulating Ion transfer and interface stability by a bulk interphase framework for stable lithium metal batteries. *Adv. Funct. Mater.* **2023**, *33*, 2303077.

[64] Aspinall, J.; Chart, Y.; Guo, H.; Shrestha, P.; Burton, M.; Pasta, M. Effect of microstructure on the cycling behavior of Li–In alloy anodes for solid-state batteries. *ACS Energy Lett.* **2024**, *9*, 578–585.

[65] Lu, B. Y.; Cheng, D. Y.; Sreenarayanan, B.; Li, W. K.; Bhamwala, B.; Bao, W.; Meng, Y. S. Key parameters in determining the reactivity of lithium metal battery. *ACS Energy Lett.* **2023**, *8*, 3230–3238.

[66] Yue, L. G.; Wang, X. Y.; Chen, L.; Shen, D. J.; Shao, Z. H.; Wu, H.; Xiao, S. F.; Liang, W. Q.; Yu, Y. J.; Li, Y. Y. *In situ* interface engineering of highly nitrogen-rich triazine-based covalent organic frameworks for an ultra-stable, dendrite-free lithium-metal anode. *Energy Environ. Sci.* **2024**, *17*, 1117–1131.

[67] Xie, C. Y.; Zhao, C.; Jeong, H.; Li, T. Y.; Li, L. X.; Xu, W. Q.; Yang, Z. Z.; Lin, C.; Liu, Q.; Cheng, L. et al. Suppressing universal cathode crossover in high-energy lithium metal batteries via a versatile interlayer design. *Angew. Chem., Int. Ed.* **2023**, *62*, e202217476.

[68] Zhang, Q. K.; Zhang, X. Q.; Wan, J.; Yao, N.; Song, T. L.; Xie, J.; Hou, L. P.; Zhou, M. Y.; Chen, X.; Li, B. Q. et al. Homogeneous and mechanically stable solid-electrolyte interphase enabled by trioxane-modulated electrolytes for lithium metal batteries. *Nat. Energy* **2023**, *8*, 725–735.

[69] Sun, Y.; Li, J. C.; Xu, S.; Zhou, H. S.; Guo, S. H. Molecular engineering toward robust solid electrolyte interphase for lithium metal batteries. *Adv. Mater.* **2024**, *36*, 2311687.

[70] Wagner-Henke, J.; Kuai, D. C.; Gerasimov, M.; Röder, F.; Balbuena, P. B.; Krewer, U. Knowledge-driven design of solid-electrolyte interphases on lithium metal via multiscale modelling. *Nat. Commun.* **2023**, *14*, 6823.

[71] Jagger, B.; Pasta, M. Solid electrolyte interphases in lithium metal batteries. *Joule* **2023**, *7*, 2228–2244.

[72] Cheng, X. B.; Yang, S. J.; Liu, Z. C.; Guo, J. X.; Jiang, F. N.; Jiang, F.; Xiong, X. S.; Tang, W. B.; Yuan, H.; Huang, J. Q. et al. Electrochemically and thermally stable inorganics-rich solid electrolyte interphase for robust lithium metal batteries. *Adv. Mater.* **2024**, *36*, 2307370.

[73] Xia, Y. C.; Zhou, P.; Kong, X.; Tian, J. K.; Zhang, W. L.; Yan, S. S.; Hou, W. H.; Zhou, H. Y.; Dong, H.; Chen, X. X. et al. Designing an asymmetric ether-like lithium salt to enable fast-cycling high-energy lithium metal batteries. *Nat. Energy* **2023**, *8*, 934–945.

[74] Zhang, Q. C.; Xu, L.; Yue, X. Y.; Liu, J. J.; Wang, X.; He, X. Y.; Shi, Z. D.; Niu, S.; Gao, W.; Cheng, C. et al. Catalytic current collector design to accelerate $LiNO_3$ decomposition for high-performing lithium metal batteries. *Adv. Energy Mater.* **2023**, *13*, 2302620.

[75] Molaiyan, P.; Abdollahifar, M.; Boz, B.; Beutl, A.; Krammer, M.; Zhang, N. X.; Tron, A.; Romio, M.; Ricci, M.; Adelung, R. et al. Optimizing current collector interfaces for efficient "anode-free" lithium metal batteries. *Adv. Funct. Mater.* **2024**, *34*, 2311301.

[76] Guan, W. Q.; Wang, T.; Liu, Y. H.; Du, H. F.; Li, S. Y.; Du, Z. Z.; Ai, W. Impact of morphological dimensions in carbon-based interlayers on lithium metal anode stabilization. *Adv. Energy Mater.* **2023**, *13*, 2302565.

[77] Xiao, P. T.; Yun, X. R.; Chen, Y. F.; Guo, X. W.; Gao, P.; Zhou, G. M.; Zheng, C. M. Insights into the solvation chemistry in liquid electrolytes for lithium-based rechargeable batteries. *Chem. Soc. Rev.* **2023**, *52*, 5255–5316.

[78] Kim, S. C.; Wang, J. Y.; Xu, R.; Zhang, P.; Chen, Y. L.; Huang, Z. J.; Yang, Y. F.; Yu, Z. A.; Oyakhire, S. T.; Zhang, W. B. et al. High-entropy electrolytes for practical lithium metal batteries. *Nat. Energy* **2023**, *8*, 814–826.

[79] Wang, Y. D.; Ke, S. W.; Qiao, G. F.; Liang, J. C.; Zhou, X. C.; Song, X. M.; Tie, Z.; Yuan, S.; Zuo, J. L.; Jin, Z. Self-assembled lithiophilic interface with abundant nickel-bis (dithiolene) sites enabling highly durable and dendrite-free lithium metal batteries. *Adv. Energy Mater.* **2024**, *14*, 2303051.

[80] Deng, L. Q.; Dong, L. T.; Wang, Z. F.; Liu, Y.; Zhan, J.; Wang, S. H.; Song, K. P.; Qi, D. Q.; Sang, Y. H.; Liu, H. et al. Asymmetrically-fluorinated electrolyte molecule design for simultaneous achieving good solvation and high inertness to enable stable lithium metal batteries. *Adv. Energy Mater.* **2024**, *14*, 2303652.

[81] Meng, Y. F.; Zhou, D.; Liu, R. L.; Tian, Y.; Gao, Y. F.; Wang, Y.; Sun, B.; Kang, F. Y.; Armand, M.; Li, B. H. et al. Designing phosphazene-derivative electrolyte matrices to enable high-voltage lithium metal batteries for extreme working conditions. *Nat. Energy* **2023**, *8*, 1023–1033.

[82] Kwon, H.; Kim, H.; Hwang, J.; Oh, W.; Roh, Y.; Shin, D.; Kim, H. T. Borate-pyran lean electrolyte-based Li-metal batteries with minimal Li corrosion. *Nat. Energy* **2023**, *9*, 57–69.

[83] Fang, S.; Wu, F. L.; Zhao, S. Q.; Zarrabeitia, M.; Kim, G. T.; Kim, J. K.; Zhou, N. G.; Passerini, S. Adaptive multi-site gradient adsorption of siloxane-based protective layers enable high performance lithium-metal batteries. *Adv. Energy Mater.* **2023**, *13*, 2302577.

[84] Cheng, Y. F.; Wang, Z. J.; Chen, J. B.; Chen, Y. M.; Ke, X.; Wu, D. J.; Zhang, Q.; Zhu, Y. M.; Yang, X. M.; Gu, M. et al. Catalytic chemistry derived artificial solid electrolyte interphase for stable lithium metal anodes working at 20 $mA \cdot cm^{-2}$ and 20 $mAh \cdot cm^{-2}$. *Angew. Chem., Int. Ed.* **2023**, *62*, e202305723.

[85] Huang, Z. J.; Lai, J. C.; Liao, S. L.; Yu, Z. A.; Chen, Y. L.; Yu, W. L.; Gong, H. X.; Gao, X.; Yang, Y. F.; Qin, J. et al. A salt-philic, solvent-phobic interfacial coating design for lithium metal electrodes. *Nat. Energy* **2023**, *8*, 577–585.

[86] Peled, E.; Menkin, S. Review—SEI: Past, present and future. *J. Electrochem. Soc.* **2017**, *164*, A1703–A1719.

[87] Wu, H. P.; Jia, H.; Wang, C. M.; Zhang, J. G.; Xu, W. Recent

progress in understanding solid electrolyte interphase on lithium metal anodes. *Adv. Energy Mater.* **2021**, *11*, 2003092.
[88] Cheng, X. B.; Zhang, R.; Zhao, C. Z.; Wei, F.; Zhang, J. G.; Zhang, Q. A review of solid electrolyte interphases on lithium metal anode. *Adv. Sci.* **2016**, *3*, 1500213.
[89] Banerjee, A.; Wang, X. F.; Fang, C. C.; Wu, E. A.; Meng, Y. S. Interfaces and interphases in all-solid-state batteries with inorganic solid electrolytes. *Chem. Rev.* **2020**, *120*, 6878–6933.
[90] Xu, L.; Tang, S.; Cheng, Y.; Wang, K. Y.; Liang, J. Y.; Liu, C.; Cao, Y. C.; Wei, F.; Mai, L. Interfaces in solid-state lithium batteries. *Joule* **2018**, *2*, 1991–2015.
[91] Liu, H.; Cheng, X. B.; Xu, R.; Zhang, X. Q.; Yan, C.; Huang, J. Q.; Zhang, Q. Plating/stripping behavior of actual lithium metal anode. *Adv. Energy Mater.* **2019**, *9*, 1902254.
[92] Xiang, Y. X.; Tao, M. M.; Zhong, G. M.; Liang, Z. T.; Zheng, G. R.; Huang, X.; Liu, X. S.; Jin, Y. T.; Xu, N. B.; Armand, M. et al. Quantitatively analyzing the failure processes of rechargeable Li metal batteries. *Sci. Adv.* **2021**, *7*, eabj3423.
[93] Xu, S. S.; Chen, K. H.; Dasgupta, N. P.; Siegel, J. B.; Stefanopoulou, A. G. Evolution of dead lithium growth in lithium metal batteries: Experimentally validated model of the apparent capacity loss. *J. Electrochem. Soc.* **2019**, *166*, A3456–A3463.
[94] Sayavong, P.; Zhang, W. B.; Oyakhire, S. T.; Boyle, D. T.; Chen, Y. L.; Kim, S. C.; Vilá, R. A.; Holmes, S. E.; Kim, M. S.; Bent, S. F. et al. Dissolution of the solid electrolyte interphase and its effects on lithium metal anode cyclability. *J. Am. Chem. Soc.* **2023**, *145*, 12342–12350.
[95] Chen, K. H.; Wood, K. N.; Kazyak, E.; LePage, W. S.; Davis, A. L.; Sanchez, A. J.; Dasgupta, N. P. Dead lithium: Mass transport effects on voltage, capacity, and failure of lithium metal anodes. *J. Mater. Chem. A* **2017**, *5*, 11671–11681.
[96] Xu, W.; Wang, J. L.; Ding, F.; Chen, X. L.; Nasybulin, E.; Zhang, Y. H.; Zhang, J. G. Lithium metal anodes for rechargeable batteries. *Energy Environ. Sci.* **2014**, *7*, 513–537.
[97] Liu, B.; Zhang, Y.; Wang, Z. L.; Ai, C. Z.; Liu, S. F.; Liu, P.; Zhong, Y.; Lin, S. W.; Deng, S. J.; Liu, Q. et al. Coupling a sponge metal fibers skeleton with *in situ* surface engineering to achieve advanced electrodes for flexible lithium-sulfur batteries. *Adv. Mater.* **2020**, *32*, 2003657.
[98] Zhang, X. D.; Guo, Z. A.; Li, X.; Liu, Q. N.; Hu, H.; Li, F. Y.; Huang, Q.; Zhang, L. Q.; Tang, Y. F.; Huang, J. Y. Cryo-ultramicrotomy enables TEM characterization of global lithium/polymer interfaces. *Energy Environ. Sci.* **2024**, *17*, 1436–1447.
[99] Hobold, G. M.; Gallant, B. M. Quantifying capacity loss mechanisms of Li metal anodes beyond inactive Li^0. *ACS Energy Lett.* **2022**, *7*, 3458–3466.
[100] Yuan, X. T.; Liu, B.; Mecklenburg, M.; Li, Y. Z. Ultrafast deposition of faceted lithium polyhedra by outpacing SEI formation. *Nature* **2023**, *620*, 86–91.
[101] Fang, C. C.; Li, J. X.; Zhang, M. H.; Zhang, Y. H.; Yang, F.; Lee, J. Z.; Lee, M. H.; Alvarado, J.; Schroeder, M. A.; Yang, Y. Y. C. et al. Quantifying inactive lithium in lithium metal batteries. *Nature* **2019**, *572*, 511–515.
[102] Sun, K.; Cao, C. T.; Zhao, D. Y.; Tong, X.; Bak, S. M.; Du, Y. H.; Wang, F.; Steingart, D. A. Degradation of lithium iron phosphate sulfide solid-state batteries by conductive interfaces. *J. Phys. Chem. C* **2023**, *127*, 19396–19405.
[103] Pei, A.; Zheng, G. Y.; Shi, F. F.; Li, Y. Z.; Cui, Y. Nanoscale nucleation and growth of electrodeposited lithium metal. *Nano Lett.* **2017**, *17*, 1132–1139.
[104] Liu, Y. H.; Li, Y. F.; Du, Z. Z.; He, C.; Bi, J. X.; Li, S. Y.; Guan, W. Q.; Du, H. F.; Ai, W. Integrated gradient Cu current collector enables bottom–up Li growth for Li metal anodes: Role of interfacial structure. *Adv. Sci.* **2023**, *10*, 2301288.
[105] Chen, X. R.; Zhao, B. C.; Yan, C.; Zhang, Q. Review on Li deposition in working batteries: From nucleation to early growth. *Adv. Mater.* **2021**, *33*, 2004128.
[106] Yan, K.; Lu, Z. D.; Lee, H. W.; Xiong, F.; Hsu, P. C.; Li, Y. Z.; Zhao, J.; Chu, S.; Cui, Y. Selective deposition and stable encapsulation of lithium through heterogeneous seeded growth. *Nat. Energy* **2016**, *1*, 16010.
[107] Xue, P.; Liu, S. R.; Shi, X. L.; Sun, C.; Lai, C.; Zhou, Y.; Sui, D.; Chen, Y. S.; Liang, J. J. A hierarchical silver-nanowire-graphene host enabling ultrahigh rates and superior long-term cycling of lithium-metal composite anodes. *Adv. Mater.* **2018**, *30*, 1804165.
[108] Ye, H.; Zheng, Z. J.; Yao, H. R.; Liu, S. C.; Zuo, T. T.; Wu, X. W.; Yin, Y. X.; Li, N. W.; Gu, J. J.; Cao, F. F. et al. Guiding uniform Li plating/stripping through lithium-aluminum alloying medium for long-life Li metal batteries. *Angew. Chem., Int. Ed.* **2019**, *58*, 1094–1099.
[109] Todeschini, M.; Da Silva Fanta, A. B.; Jensen, F.; Wagner, J. B.; Han, A. P. Influence of Ti and Cr adhesion layers on ultrathin Au films. *ACS Appl. Mater. Interfaces* **2017**, *9*, 37374–37385.
[110] Chen, X. R.; Chen, X.; Yan, C.; Zhang, X. Q.; Zhang, Q.; Huang, J. Q. Role of lithiophilic metal sites in lithium metal anodes. *Energy Fuels* **2021**, *35*, 12746–12752.
[111] Chen, X. R.; Li, B. Q.; Zhao, C. X.; Zhang, R.; Zhang, Q. Synergetic coupling of lithiophilic sites and conductive scaffolds for dendrite-free lithium metal anodes. *Small Methods* **2020**, *4*, 1900177.
[112] Ma, J. J.; Yang, J. L.; Wu, C.; Huang, M.; Zhu, J. W.; Zeng, W. H.; Li, L.; Li, P.; Zhao, X.; Qiao, F. et al. Stabilizing nucleation seeds in Li metal anode via ion-selective graphene oxide interfaces. *Energy Storage Mater.* **2023**, *56*, 572–581.
[113] Wang, Y. X.; Liu, Y. J.; Nguyen, M.; Cho, J.; Katyal, N.; Vishnugopi, B. S.; Hao, H. C.; Fang, R. Y.; Wu, N.; Liu, P. C. et al. Stable anode-free all-solid-state lithium battery through tuned metal wetting on the copper current collector. *Adv. Mater.* **2023**, *35*, 2206762.
[114] Sandoval, S. E.; Lewis, J. A.; Vishnugopi, B. S.; Nelson, D. L.; Schneider, M. M.; Cortes, F. J. Q.; Matthews, C. M.; Watt, J.; Tian, M. K.; Shevchenko, P. et al. Structural and electrochemical evolution of alloy interfacial layers in anode-free solid-state batteries. *Joule* **2023**, *7*, 2054–2073.
[115] Li, Q. W.; Liu, Y. L.; Zhang, Z. H.; Chen, J. J.; Yang, Z. L.; Deng, Q. B.; Mumyatov, A. V.; Troshin, P. A.; He, G.; Hu, N. Construction of dynamic alloy interfaces for uniform Li deposition in Li-metal batteries. *Energy Environ. Mater.* **2024**, *7*, e12618.
[116] He, R. H.; Wang, Y. T.; Zhang, C. Y.; Liu, Z. H.; He, P.; Hong, X. F.; Yu, R. H.; Zhao, Y.; Wu, J. S.; Zhou, L. et al. Sequential and dendrite-free Li plating on Cu foil enabled by an ultrathin yolk–shell SiO_x/C@C layer. *Adv. Energy Mater.* **2023**, *13*, 2204075.
[117] Li, B. Q.; Chen, X. R.; Chen, X.; Zhao, C. X.; Zhang, R.; Cheng, X. B.; Zhang, Q. Favorable lithium nucleation on lithiophilic framework porphyrin for dendrite-free lithium metal anodes. *Research* **2019**, *2019*, 4608940.
[118] Zou, P. C.; Wang, C. Y.; Qin, J. Y.; Zhang, R.; Xin, H. L. A reactive wetting strategy improves lithium metal reversibility. *Energy Storage Mater.* **2023**, *58*, 176–183.
[119] Liu, L.; Wang, J. H. Overcoming copper substrate thermodynamic limitations in anode-free lithium pouch cells via *in situ* seed implantation. *Nano Lett.* **2023**, *23*, 10251–10258.
[120] Wang, J. P.; Lang, F.; Li, Q. *In situ* tailoring solid electrolyte interphase of three-dimensional Li metal electrode for enhanced Coulombic efficiency. *EcoMat* **2023**, *5*, e12354.
[121] Zhang, W. D.; Fan, Q. X.; Zhang, D. M.; Liu, L. H.; Liu, S.; Fang, Z. Y.; Li, W.; Li, X. D.; Li, M. C. Dynamic charge modulate lithium uniform plating functional composite anode for dendrite-free lithium metal batteries. *Nano Energy* **2022**, *102*, 107677.
[122] Wu, Z. H.; Wang, C. Y.; Hui, Z. Y.; Liu, H. D.; Wang, S.; Yu, S. C.; Xing, X.; Holoubek, J.; Miao, Q. S.; Xin, H. L. et al. Growing single-crystalline seeds on lithiophobic substrates to enable fast-charging lithium-metal batteries. *Nat. Energy* **2023**, *8*, 340–350.
[123] Kim, S.; Park, G.; Lee, S. J.; Seo, S.; Ryu, K.; Kim, C. H.; Choi, J. W. Lithium-metal batteries: From fundamental research to industrialization. *Adv. Mater.* **2023**, *35*, 2206625.
[124] Oyakhire, S. T.; Zhang, W. B.; Shin, A.; Xu, R.; Boyle, D. T.; Yu, Z. A.; Ye, Y. S.; Yang, Y. F.; Raiford, J. A.; Huang, W. et al.

Electrical resistance of the current collector controls lithium morphology. *Nat. Commun.* **2022**, *13*, 3986.
[125] Hu, Y. H.; Li, H.; Chen, Z. D.; Cen, W. L.; Wang, Q.; Chen, Y. G.; Davoodi, A.; Liu, W. Li-alloy texture creates in-built Li (110) epitaxy in a thin Li-metal anode allowing high depth-of-discharge cycling in carbonate electrolyte. *Chem. Eng. J.* **2023**, *466*, 143084.
[126] Kim, M. H.; Kim, D. Y.; Li, Y. Q.; Seo, J.; Kim, J.; Kim, M. S.; Kim, M.; Kim, T.; Jung, U.; Park, S. W. et al. A single-crystal copper (111) current collector for anode-free lithium batteries [Online]. 2022. https://chemrxiv.org/engage/chemrxiv/article-details/63949e6704bc6663b910730b (accessed Apr 1, 2024).
[127] Zhang, Y. H.; Zhao, P. Y.; Nie, Q. N.; Li, Y.; Guo, R.; Hong, Y. F.; Deng, J. K.; Song, J. X. Enabling 420 $Wh \cdot kg^{-1}$ stable lithium-metal pouch cells by lanthanum doping. *Adv. Mater.* **2023**, *35*, 2211032.
[128] Lai, G. M.; Jiao, J. Y.; Fang, C.; Jiang, Y.; Sheng, L. Y.; Xu, B.; Ouyang, C. Y.; Zheng, J. X. The mechanism of Li deposition on the cu substrates in the anode-free Li metal batteries. *Small* **2023**, *19*, 2205416.
[129] Ishikawa, K.; Ito, Y.; Harada, S.; Tagawa, M.; Ujihara, T. Crystal orientation dependence of precipitate structure of electrodeposited Li metal on Cu current collectors. *Cryst. Growth Des.* **2017**, *17*, 2379–2385.
[130] Ishikawa, K.; Harada, S.; Tagawa, M.; Ujihara, T. Effect of crystal orientation of Cu current collectors on cycling stability of Li metal anodes. *ACS Appl. Mater. Interfaces* **2020**, *12*, 9341–9346.
[131] Kim, Y. J.; Kwon, S. H.; Noh, H.; Yuk, S.; Lee, H.; Jin, H. S.; Lee, J.; Zhang, J. G.; Lee, S. G.; Guim, H. et al. Facet selectivity of Cu current collector for Li electrodeposition. *Energy Storage Mater.* **2019**, *19*, 154–162.
[132] Gu, Y.; Xu, H. Y.; Zhang, X. G.; Wang, W. W.; He, J. W.; Tang, S.; Yan, J. W.; Wu, D. Y.; Zheng, M. S.; Dong, Q. F. et al. Lithiophilic faceted Cu (100) surfaces: High utilization of host surface and cavities for lithium metal anodes. *Angew. Chem., Int. Ed.* **2019**, *58*, 3092–3096.
[133] Luo, P.; Wolf, S. E.; Govind, S.; Stephens, R. B.; Kim, D. H.; Chen, C. Y.; Nguyen, T.; Wąsik, P.; Zhernenkov, M.; McClimon, B. et al. High-density stable glasses formed on soft substrates. *Nat. Mater.* **2024**, *23*, 688–694.
[134] Wang, X.; Zeng, W.; Hong, L.; Xu, W. W.; Yang, H. K.; Wang, F.; Duan, H. G.; Tang, M.; Jiang, H. Q. Stress-driven lithium dendrite growth mechanism and dendrite mitigation by electroplating on soft substrates. *Nat. Energy* **2018**, *3*, 227–235.
[135] Oh, J.; Choi, S. H.; Kim, J. Y.; Lee, J.; Lee, T.; Lee, N.; Lee, T.; Sohn, Y.; Chung, W. J.; Bae, K. Y. et al. Anode-less all-solid-state batteries operating at room temperature and low pressure. *Adv. Energy Mater.* **2023**, *13*, 2301508.
[136] Tang, Y. P.; Shen, K.; Lv, Z. Y.; Xu, X.; Hou, G. Y.; Cao, H. Z.; Wu, L. K.; Zheng, G. Q.; Deng, Y. D. Three-dimensional ordered macroporous Cu current collector for lithium metal anode: Uniform nucleation by seed crystal. *J. Power Sources* **2018**, *403*, 82–89.
[137] Brissot, C.; Rosso, M.; Chazalviel, J. N.; Baudry, P.; Lascaud, S. *In situ* study of dendritic growth inlithium/PEO-salt/lithium cells. *Electrochim. Acta* **1998**, *43*, 1569–1574.
[138] Li, Q.; Zhu, S. P.; Lu, Y. Y. 3D porous Cu current collector/Li-metal composite anode for stable lithium-metal batteries. *Adv. Funct. Mater.* **2017**, *27*, 1606422.
[139] Yang, C. P.; Yin, Y. X.; Zhang, S. F.; Li, N. W.; Guo, Y. G. Accommodating lithium into 3D current collectors with a submicron skeleton towards long-life lithium metal anodes. *Nat. Commun.* **2015**, *6*, 8058.
[140] Ingber, T. T. K.; Bela, M. M.; Püttmann, F.; Dohmann, J. F.; Bieker, P.; Börner, M.; Winter, M.; Stan, M. C. Elucidating the lithium deposition behavior in open-porous copper micro-foam negative electrodes for zero-excess lithium metal batteries. *J. Mater. Chem. A* **2023**, *11*, 17828–17840.
[141] Zhang, W. Y.; Li, J. L.; Chen, H. X.; Jin, H. X.; Li, P.; Zhang, Y. J.; Xu, C.; Zhao, S. M.; Du, Y. Q.; Zhang, J. X. Natural template-derived 3D porous current collector for dendrite-free lithium metal battery. *Nano* **2020**, *15*, 2050033.
[142] Wang, Y. Y.; Wang, Z. J.; Lei, D. N.; Lv, W.; Zhao, Q.; Ni, B.; Liu, Y.; Li, B. H.; Kang, F. Y.; He, Y. B. Spherical Li deposited inside 3D Cu skeleton as anode with ultrastable performance. *ACS Appl. Mater. Interfaces* **2018**, *10*, 20244–20249.
[143] Umh, H. N.; Park, J.; Yeo, J.; Jung, S.; Nam, I.; Yi, J. Lithium metal anode on a copper dendritic superstructure. *Electrochem. Commun.* **2019**, *99*, 27–31.
[144] Adair, K. R.; Iqbal, M.; Wang, C. H.; Zhao, Y.; Banis, M. N.; Li, R. Y.; Zhang, L.; Yang, R.; Lu, S. G.; Sun, X. L. Towards high performance Li metal batteries: Nanoscale surface modification of 3D metal hosts for pre-stored Li metal anodes. *Nano Energy* **2018**, *54*, 375–382.
[145] Lin, K.; Xu, X. F.; Qin, X. Y.; Zhang, G. Q.; Liu, M.; Lv, F. Z.; Xia, Y.; Kang, F. Y.; Chen, G. H.; Li, B. H. Restructured rimous copper foam as robust lithium host. *Energy Storage Mater.* **2020**, *26*, 250–259.
[146] Park, S. K.; Copic, D.; Zhao, T. Z.; Rutkowska, A.; Wen, B.; Sanders, K.; He, R. H.; Kim, H. K.; De Volder, M. 3D porous Cu-composites for stable Li-metal battery anodes. *ACS Nano* **2023**, *17*, 14658–14666.
[147] Yang, I.; Jeong, J. H.; Seok, J. Y.; Kim, S. Structurally tailored hierarchical Cu current collector with selective inward growth of lithium for high-performance lithium metal batteries. *Adv. Energy Mater.* **2023**, *13*, 2202321.
[148] Liu, H.; Wang, E. R.; Zhang, Q.; Ren, Y. B.; Guo, X. W.; Wang, L.; Li, G. Y.; Yu, H. J. Unique 3D nanoporous/macroporous structure Cu current collector for dendrite-free lithium deposition. *Energy Storage Mater.* **2019**, *17*, 253–259.
[149] Yun, Q. B.; He, Y. B.; Lv, W.; Zhao, Y.; Li, B. H.; Kang, F. Y.; Yang, Q. H. Chemical dealloying derived 3D porous current collector for Li metal anodes. *Adv. Mater.* **2016**, *28*, 6932–6939.
[150] Wu, S. L.; Jiao, T. P.; Yang, S. R.; Liu, B.; Zhang, W. J.; Zhang, K. L. Lithiophilicity conversion of the Cu surface through facile thermal oxidation: Boosting a stable Li–Cu composite anode through melt infusion. *J. Mater. Chem. A* **2019**, *7*, 5726–5732.
[151] Fan, H. L.; Gao, C. H.; Dong, Q. Y.; Hong, B.; Fang, Z.; Hu, M. Y.; Lai, Y. Q. Silver sites guide spatially homogeneous plating of lithium metal in 3D host. *J. Electroanal. Chem.* **2018**, *824*, 175–180.
[152] Li, Z. H.; He, Q.; Zhou, C.; Li, Y.; Liu, Z. H.; Hong, X. F.; Xu, X.; Zhao, Y.; Mai, L. Rationally design lithiophilic surfaces toward high-energy Lithium metal battery. *Energy Storage Mater.* **2021**, *37*, 40–46.
[153] Wang, J.; Li, L. G.; Hu, H. M.; Hu, H. F.; Guan, Q. H.; Huang, M.; Jia, L. J.; Adenusi, H.; Tian, K. V.; Zhang, J. et al. Toward dendrite-free metallic lithium anodes: From structural design to optimal electrochemical diffusion kinetics. *ACS Nano* **2022**, *16*, 17729–17760.
[154] Zhang, X. Q.; Chen, X.; Xu, R.; Cheng, X. B.; Peng, H. J.; Zhang, R.; Huang, J. Q.; Zhang, Q. Columnar lithium metal anodes. *Angew. Chem., Int. Ed.* **2017**, *56*, 14207–14211.
[155] Johnson, B. A.; White, R. E. Characterization of commercially available lithium-ion batteries. *J. Power Sources* **1998**, *70*, 48–54.
[156] Liu, S.; Wang, A. X.; Li, Q. Q.; Wu, J. S.; Chiou, K.; Huang, J. X.; Luo, J. Y. Crumpled graphene balls stabilized dendrite-free lithium metal anodes. *Joule* **2018**, *2*, 184–193.
[157] Zhang, F.; Liu, P.; Tian, Y.; Wu, J. F.; Wang, X. W.; Li, H. L.; Liu, X. Y. Uniform lithium nucleation/deposition regulated by N/S co-doped carbon nanospheres towards ultra-stable lithium metal anodes. *J. Mater. Chem. A* **2022**, *10*, 1463–1472.
[158] Zhang, Y.; Liu, B. Y.; Hitz, E.; Luo, W.; Yao, Y. G.; Li, Y. J.; Dai, J. Q.; Chen, C. J.; Wang, Y. B.; Yang, C. P. et al. A carbon-based 3D current collector with surface protection for Li metal anode. *Nano Res.* **2017**, *10*, 1356–1365.
[159] Wang, H. S.; Li, Y. Z.; Li, Y. B.; Liu, Y. Y.; Lin, D. C.; Zhu, C.; Chen, G. X.; Yang, A. K.; Yan, K.; Chen, H. et al. Wrinkled graphene cages as hosts for high-capacity Li metal anodes shown by cryogenic electron microscopy. *Nano Lett.* **2019**, *19*, 1326–1335.
[160] Song, W. X.; Cui, S. Q.; Zhang, J. J.; Fan, S. Z.; Chen, L. L.; Zhang, H. M.; Zhang, Y. T.; Meng, X. M. Three-dimensional carbon foam modified with Mg_3N_2 for ultralong cyclability of a

dendrite-free Li metal anode. *ACS Appl. Mater. Interfaces* **2023**, *15*, 9421–9430.
[161] Yang, T. Y.; Li, L.; Zhao, T.; Ye, Y. S.; Ye, Z. Q.; Xu, S. N.; Wu, F.; Chen, R. J. From flower-like to spherical deposition: A GCNT aerogel scaffold for fast-charging lithium metal batteries. *Adv. Energy Mater.* **2021**, *11*, 2102454.
[162] Pan, D.; Zhao, C. L.; Qi, X. G.; Liu, L. L.; Rong, X. H.; Sun, S. W.; Lu, Y. X.; Bai, Y.; Hu, Y. S. Defect-abundant commercializable 3D carbon papers for fabricating composite Li anode with high loading and long life. *Energy Storage Mater.* **2022**, *50*, 407–416.
[163] Acebedo, B.; Morant-Miñana, M. C.; Gonzalo, E.; De Larramendi, I. R.; Villaverde, A.; Rikarte, J.; Fallarino, L. Current status and future perspective on lithium metal anode production methods. *Adv. Energy Mater.* **2023**, *13*, 2203744.
[164] Boyle, D. T.; Kim, S. C.; Oyakhire, S. T.; Vilá, R. A.; Huang, Z. J.; Sayavong, P.; Qin, J.; Bao, Z. N.; Cui, Y. Correlating kinetics to cyclability reveals thermodynamic origin of lithium anode morphology in liquid electrolytes. *J. Am. Chem. Soc.* **2022**, *144*, 20717–20725.
[165] Bai, P.; Li, J.; Brushett, F. R.; Bazant, M. Z. Transition of lithium growth mechanisms in liquid electrolytes. *Energy Environ. Sci.* **2016**, *9*, 3221–3229.
[166] Zhang, Y. H.; Qian, J. F.; Xu, W.; Russell, S. M.; Chen, X. L.; Nasybulin, E.; Bhattacharya, P.; Engelhard, M. H.; Mei, D. H.; Cao, R. G. et al. Dendrite-free lithium deposition with self-aligned nanorod structure. *Nano Lett.* **2014**, *14*, 6889–6896.
[167] Zhang, W. D.; Wu, Q.; Huang, J. X.; Fan, L.; Shen, Z. Y.; He, Y.; Feng, Q.; Zhu, G. N.; Lu, Y. Y. Colossal granular lithium deposits enabled by the grain-coarsening effect for high-efficiency lithium metal full batteries. *Adv. Mater.* **2020**, *32*, 2001740.
[168] Zhou, S.; Zhang, Y. F.; Chai, S. M.; Usman, I.; Qiao, Y.; Luo, S. Z.; Xie, X. F.; Chen, J.; Liang, S. Q.; Pan, A. Q. et al. Incorporation of LiF into functionalized polymer fiber networks enabling high capacity and high rate cycling of lithium metal composite anodes. *Chem. Eng. J.* **2021**, *404*, 126508.
[169] Kim, S.; Lee, J. A.; Lee, T. K.; Baek, K.; Kim, J.; Kim, B.; Byun, J. H.; Lee, H. W.; Kang, S. J.; Choi, J. A. et al. Wide-temperature-range operation of lithium-metal batteries using partially and weakly solvating liquid electrolytes. *Energy Environ. Sci.* **2023**, *16*, 5108–5122.
[170] Ma, T.; Ni, Y. X.; Wang, Q. R.; Zhang, W. J.; Jin, S.; Zheng, S. B.; Yang, X.; Hou, Y. P.; Tao, Z. L.; Chen, J. Optimize lithium deposition at low temperature by weakly solvating power solvent. *Angew. Chem., Int. Ed.* **2022**, *61*, e202207927.
[171] Wang, Q. D.; Zhao, C. L.; Wang, S. W.; Wang, J. L.; Liu, M.; Ganapathy, S.; Bai, X. D.; Li, B. H.; Wagemaker, M. Clarifying the relationship between the lithium deposition coverage and microstructure in lithium metal batteries. *J. Am. Chem. Soc.* **2022**, *144*, 21961–21971.
[172] Chen, Y. W.; Li, M. H.; Liu, Y.; Jie, Y. L.; Li, W. X.; Huang, F. Y.; Li, X. P.; He, Z. X.; Ren, X. D.; Chen, Y. H. et al. Origin of dendrite-free lithium deposition in concentrated electrolytes. *Nat. Commun.* **2023**, *14*, 2655.
[173] Aarts, M.; Patnaik, S. G.; Van Roy, T.; Sergeant, S.; Debucquoy, M.; Vereecken, P. M. Water as additive directing lithium electrodeposition. *ACS Energy Lett.* **2024**, *9*, 513–519.
[174] Zhang, X. Z.; Xu, P.; Duan, J. N.; Lin, X. D.; Sun, J. J.; Shi, W. J.; Xu, H. W.; Dou, W. J.; Zheng, Q. Y.; Yuan, R. M. et al. A dicarbonate solvent electrolyte for high performance 5 V-class lithium-based batteries. *Nat. Commun.* **2024**, *15*, 536.
[175] Zeng, H. P.; Yu, K.; Li, J. W.; Yuan, M. M.; Wang, J. J.; Wang, Q. R.; Lai, A. J.; Jiang, Y. D.; Yan, X.; Zhang, G. Z. et al. Beyond LiF: Tailoring Li_2O-dominated solid electrolyte interphase for stable lithium metal batteries. *ACS Nano* **2024**, *18*, 1969–1981.
[176] Lu, Y.; Zhang, W. L.; Liu, S. Z.; Cao, Q. B.; Yan, S. S.; Liu, H.; Hou, W. H.; Zhou, P.; Song, X.; Ou, Y. et al. Tuning the Li^+ solvation structure by a "bulky coordinating" strategy enables nonflammable electrolyte for ultrahigh voltage lithium metal batteries. *ACS Nano* **2023**, *17*, 9586–9599.
[177] Cheng, L. W.; Wang, Y. Y.; Yang, J.; Tang, M. Y.; Zhang, C. G.; Zhu, Q. N.; Wang, S. C.; Li, Y. T.; Hu, P. F.; Wang, H. An ultrafast and stable Li-metal battery cycled at −40 °C. *Adv. Funct. Mater.* **2023**, *33*, 2212349.
[178] Ma, T.; Ni, Y. X.; Wang, Q. R.; Xiao, J.; Huang, Z. X.; Tao, Z. L.; Chen, J. Lithium dendrites inhibition by regulating electrodeposition kinetics. *Energy Storage Mater.* **2022**, *52*, 69–75.
[179] Boyle, D. T.; Li, Y. Z.; Pei, A.; Vilá, R. A.; Zhang, Z. W.; Sayavong, P.; Kim, M. S.; Huang, W.; Wang, H. X.; Liu, Y. Z. et al. Resolving current-dependent regimes of electroplating mechanisms for fast charging lithium metal anodes. *Nano Lett.* **2022**, *22*, 8224–8232.
[180] Zhu, J. Q.; Cui, Z.; Wang, H.; Zhang, L. J.; Liu, Q.; Lu, A. J.; Ji, T.; Hu, J. Q.; Luo, W.; Zou, R. J. A protection route based on the dual-mode transfer of lithium ions for lithiophilic site during the nucleation period. *Adv. Energy Mater.* **2023**, *13*, 2302687.
[181] Weber, R.; Genovese, M.; Louli, A. J.; Hames, S.; Martin, C.; Hill, I. G.; Dahn, J. R. Long cycle life and dendrite-free lithium morphology in anode-free lithium pouch cells enabled by a dual-salt liquid electrolyte. *Nat. Energy* **2019**, *4*, 683–689.
[182] Kazyak, E.; Wang, M. J.; Lee, K.; Yadavalli, S.; Sanchez, A. J.; Thouless, M. D.; Sakamoto, J.; Dasgupta, N. P. Understanding the electro-chemo-mechanics of Li plating in anode-free solid-state batteries with *operando* 3D microscopy. *Matter* **2022**, *5*, 3912–3934.
[183] Fincher, C. D.; Athanasiou, C. E.; Gilgenbach, C.; Wang, M.; Sheldon, B. W.; Carter, W. C.; Chiang, Y. M. Controlling dendrite propagation in solid-state batteries with engineered stress. *Joule* **2022**, *6*, 2794–2809.
[184] Yin, X. S.; Tang, W.; Jung, I. D.; Phua, K. C.; Adams, S.; Lee, S. W.; Zheng, G. W. Insights into morphological evolution and cycling behaviour of lithium metal anode under mechanical pressure. *Nano Energy* **2018**, *50*, 659–664.
[185] Lee, H.; Chen, S. R.; Ren, X. D.; Martinez, A.; Shutthanandan, V.; Vijayakumar, M.; Han, K. S.; Li, Q. Y.; Liu, J.; Xu, W. et al. Electrode edge effects and the failure mechanism of lithium-metal batteries. *ChemSusChem* **2018**, *11*, 3821–3828.
[186] Kim, H.; Lee, S. H.; Kim, J. M.; Yoon, C. S.; Sun, Y. K. High-energy-density, long-life Li-metal batteries via application of external pressure. *ACS Energy Lett.* **2023**, *8*, 2970–2978.
[187] Fang, C. C.; Lu, B. Y.; Pawar, G.; Zhang, M. H.; Cheng, D. Y.; Chen, S. R.; Ceja, M.; Doux, J. M.; Musrock, H.; Cai, M. et al. Pressure-tailored lithium deposition and dissolution in lithium metal batteries. *Nat. Energy* **2021**, *6*, 987–994.
[188] Kalnaus, S.; Dudney, N. J.; Westover, A. S.; Herbert, E.; Hackney, S. Solid-state batteries: The critical role of mechanics. *Science* **2023**, *381*, eabg5998.
[189] Lee, C.; Kim, J. Y.; Bae, K. Y.; Kim, T.; Jung, S. J.; Son, S.; Lee, H. W. Enhancing electrochemomechanics: How stack pressure regulation affects all-solid-state batteries. *Energy Storage Mater.* **2024**, *66*, 103196.
[190] Qin, J. L.; Pei, F.; Wang, R.; Wu, L.; Han, Y.; Xiao, P.; Shen, Y.; Yuan, L. X.; Huang, Y. H.; Wang, D. L. Sulfur vacancies and 1T phase-rich MoS_2 nanosheets as an artificial solid electrolyte interphase for 400 $Wh \cdot kg^{-1}$ lithium metal batteries. *Adv. Mater.* **2024**, *36*, 2312773.
[191] Lin, L.; Yue, K.; Xia, L.; Yan, X. L.; Zheng, H. F.; Zhang, Y. G.; Sa, B.; Li, J. J.; Wang, L. S.; Lin, J. et al. Tailoring Li deposition by regulating structural connectivity of electrochemical Li reservoir in Li-metal batteries. *Angew. Chem., Int. Ed.* **2024**, *63*, e202319847.
[192] Park, H.; Jeon, Y.; Chung, W. J.; Bae, Y.; Kim, J.; Baek, H.; Park, J. Early stage Li plating by liquid phase and cryogenic transmission electron microscopy. *ACS Energy Lett.* **2023**, *8*, 715–721.
[193] Wang, C. Y.; Lin, R. Q.; He, Y. B.; Zou, P. C.; Kisslinger, K.; He, Q.; Li, J.; Xin, H. L. Tension-induced cavitation in Li-metal stripping. *Adv. Mater.* **2023**, *35*, 2209091.
[194] Sun, Z. H.; Wang, Y. K.; Shen, S. Y.; Li, X. Y.; Hu, X. F.; Hu, M. Y.; Su, Y. Q.; Ding, S. J.; Xiao, C. H. Directing (110) oriented lithium deposition through high-flux solid electrolyte interphase for dendrite-free lithium metal batteries. *Angew. Chem., Int. Ed.* **2023**, *62*, e202309622.
[195] Zhao, Y.; Ye, H. L.; Zhang, H. Y.; Zhao, D.; Huang, L. M.; Lee, J. Y. The beneficial effects of black phosphorous modification of the

anode current collector in Li-metal free Li_2S-based batteries. *Mater. Today Energy* **2022**, *30*, 101179.

[196] Wi, T. U.; Park, S. O.; Yeom, S. J.; Kim, M. H.; Kristanto, I.; Wang, H. T.; Kwak, S. K.; Lee, H. W. Revealing the dual-layered solid electrolyte interphase on lithium metal anodes via cryogenic electron microscopy. *ACS Energy Lett.* **2023**, *8*, 2193–2200.

[197] Zhang, D.; Dai, A.; Wu, M.; Shen, K.; Xiao, T.; Hou, G. Y.; Lu, J.; Tang, Y. P. Lithiophilic 3D porous CuZn current collector for stable lithium metal batteries. *ACS Energy Lett.* **2020**, *5*, 180–186.

[198] Liu, F.; Xu, R.; Wu, Y. C.; Boyle, D. T.; Yang, A. K.; Xu, J. W.; Zhu, Y. Y.; Ye, Y. S.; Yu, Z. A.; Zhang, Z. W. et al. Dynamic spatial progression of isolated lithium during battery operations. *Nature* **2021**, *600*, 659–663.

[199] Han, Y. H.; Jie, Y. L.; Huang, F. Y.; Chen, Y. W.; Lei, Z. W.; Zhang, G. Q.; Ren, X. D.; Qin, L. J.; Cao, R. G.; Jiao, S. H. Enabling stable lithium metal anode through electrochemical kinetics manipulation. *Adv. Funct. Mater.* **2019**, *29*, 1904629.

[200] Wang, J. Y.; Huang, W.; Pei, A.; Li, Y. Z.; Shi, F. F.; Yu, X. Y.; Cui, Y. Improving cyclability of Li metal batteries at elevated temperatures and its origin revealed by cryo-electron microscopy. *Nat. Energy* **2019**, *4*, 664–670.

[201] Li, Y. J.; Mao, E. Y.; Min, Z. W.; Cai, Z.; Chen, Z. H.; Fu, L.; Duan, X. R.; Wang, L. Y.; Zhang, C.; Lu, Z. H. et al. Hybrid polymer-alloy-fluoride interphase enabling fast ion transport kinetics for low-temperature lithium metal batteries. *ACS Nano* **2023**, *17*, 19459–19469.

[202] Tao, M. M.; Chen, X. X.; Lin, H. X.; Jin, Y. T.; Shan, P. Z.; Zhao, D. H.; Gao, M. B.; Liang, Z. T.; Yang, Y. Clarifying the temperature-dependent lithium deposition/stripping process and the evolution of inactive Li in lithium metal batteries. *ACS Nano* **2023**, *17*, 24104–24114.

[203] Heenan, T. M. M.; Mombrini, I.; Llewellyn, A.; Checchia, S.; Tan, C.; Johnson, M. J.; Jnawali, A.; Garbarino, G.; Jervis, R.; Brett, D. J. L. et al. Mapping internal temperatures during high-rate battery applications. *Nature* **2023**, *617*, 507–512.